Research

New Phytologist

Meiotic instability and irregular chromosome pairing underpin heat-induced infertility in bread wheat carrying the *Rht-B1b* or *Rht-D1b* Green Revolution genes

András Cseh[1], Andrea Lenykó-Thegze[1,2], Diána Makai[1], Fanni Szabados[1], Kamirán Áron Hamow[1], Zsolt Gulyás[1], Tibor Kiss[1,3], Ildikó Karsai[1], Blanka Moncsek[1], Edit Mihók[1] and Adél Sepsi[1]

[1]HUN-REN, Centre for Agricultural Research, 2462, Martonvásár, Brunszvik u. 2, Hungary; [2]Doctoral School of Biology, Institute of Biology, ELTE Eötvös Loránd University, Egyetem tér 1-3, Budapest, 1053, Hungary; [3]Food and Wine Research Institute, Eszterházy Károly Catholic University, Eszterházy tér 1, Eger, 3300, Hungary

Author for correspondence:
Adél Sepsi
Email: sepsi.adel@atk.hun-ren.hu

Received: *28 February 2023*
Accepted: *12 August 2023*

New Phytologist (2024) **241:** 180–196
doi: 10.1111/nph.19256

Key words: bread wheat (*Triticum aestivum*), chromosome synapsis, climate change, gibberellic acid, heat stress, meiosis, recombination, *Rht-B1b* and *Rht-D1b* dwarfing genes.

Summary

- Mutations in the *Rht-B1a* and *Rht-D1a* genes of wheat (*Triticum aestivum*; resulting in *Rht-B1b* and *Rht-D1b* alleles) cause gibberellin-insensitive dwarfism and are one of the most important elements of increased yield introduced during the 'Green Revolution'.
- We measured the effects of a short period of heat imposed during the early reproductive stage on near-isogenic lines carrying *Rht-B1b* or *Rht-D1b* alleles, with respect to the wild-type (WT).
- The temperature shift caused a significant fertility loss within the ears of *Rht-B1b* and *Rht-D1b* wheats, greater than that observed for the WT. Defects in chromosome synapsis, reduced homologous recombination and a high frequency of chromosome mis-segregation were associated with reduced fertility. The transcription of *TaGA3ox* gene involved in the final stage of gibberellic acid (GA) biosynthesis was activated and ultra-performance liquid chromatography–tandem mass spectrometry identified GA_1 as the dominant bioactive GA in developing ears, but levels were unaffected by the elevated temperature.
- *Rht-B1b* and *Rht-D1b* mutants were inclined to meiotic errors under optimal temperatures and showed a higher susceptibility to heat than their tall counterparts. Identification and introduction of new dwarfing alleles into modern breeding programmes is invaluable in the development of climate-resilient wheat varieties.

Introduction

Bread wheat (*Triticum aestivum*) is one of our major food commodities, with a global production rate close to 1 billion tonnes per year and a world trade greater than any other crops (FAOSTAT, http://www.fao.org/faostat). The high yield performance of today's wheats greatly relies on their semidwarf stature, whereby the reduced stem elongation is associated with an improved resistance to lodging and a higher number of grains per spike (Borner *et al.*, 1993; Miralles *et al.*, 1998).

The semidwarf growth habit is known to be largely controlled by mutant alleles of the reduced height (*Rht*) genes, introduced into modern wheat varieties during the Green Revolution (1950s). The *Rht-B1b* and *Rht-D1b* alleles encode truncated repressor proteins termed as DELLAs that counteract the effect of the growth stimulant plant hormone gibberellic acid (GA) via transcriptional regulation (Hedden, 2003; Lumpkin, 2015). Wild-type (WT) DELLAs are proteolytically degraded in the presence of GA, if it binds its soluble receptor protein GIBBERELLIN-INSENSITIVE DWARF1 (GID1). Mutated DELLAs, however, are resistant to GA-GID1-dependent proteolysis and thus exert a permanent growth repression (Peng *et al.*, 1999; Wu *et al.*, 2011; Van De Velde *et al.*, 2021).

The yield benefits of gibberellin-insensitive semidwarfs rely on optimal growth conditions (Rebetzke *et al.*, 2014; Jatayev *et al.*, 2020; Ingvordsen *et al.*, 2022). Warm temperatures reduce wheat productivity by affecting almost all aspects of reproductive development. For instance, meiosis, the specialised cell division responsible for functional gamete formation, has a strict requirement for temperature (Bayliss & Riley, 1972; De Storme & Geelen, 2014; Bomblies *et al.*, 2015), with the early stages being particularly heat-sensitive (Bennett *et al.*, 1973; Draeger & Moore, 2017). At prophase I, stage of early meiosis, maternal and paternal homologous chromosomes mutually recognise each other, juxtapose by the proteinaceous structure of the synaptonemal complex (SC) and exchange parts of their genetic material via DNA crossing over (Schwarzacher, 2003; Osman *et al.*, 2011; Mercier *et al.*, 2015; Zickler & Kleckner, 2015). In addition to ensuring genetic diversity, meiotic recombination by crossovers (COs) is essential for creating physical connections between the homologous chromosomes, cytologically termed as chiasmata, which are central to balanced chromosome segregation in

anaphase I (Hunter, 2015; Lambing *et al.*, 2017). Recombination is initiated by a large number of programmed double-strand breaks (DSBs), which can be repaired by CO- or noncrossover (NCO) pathways (Grelon *et al.*, 2001; Hartung *et al.*, 2007; Drouaud *et al.*, 2013; Benyahya *et al.*, 2020). CO designation is regulated by multiple mechanisms with the SC playing a central role (Barakate *et al.*, 2014; Higgins *et al.*, 2014; Woglar & Villeneuve, 2018; Durand *et al.*, 2022). In leptotene (the first substage of meiotic prophase) concomitant with DSB initiation, axial element (AE) proteins are loaded into the chromosome axes (Armstrong *et al.*, 2002; Phillips *et al.*, 2012; Hesse *et al.*, 2019; Lambing *et al.*, 2020). Subsequently, in zygotene AEs become interconnected by transverse filament proteins giving rise to the central element (CE) of the SC (Higgins *et al.*, 2005; Osman *et al.*, 2006; Khoo *et al.*, 2012). In cereals, the SC is initially polymerised starting from the subtelomeric regions and progressing towards the interstitial regions of the chromosomes (Higgins *et al.*, 2012), and interstitial synapsis elongates later from multiple chromosomal sites (Lenykó-Thegze *et al.*, 2021). A meiosis-specific chromatin dynamics is involved in creating a spatially polarised chromatin organisation before SC initiation in wheat (Sepsi & Schwarzacher, 2020). Telomeres become associated at the nuclear periphery and form the telomere bouquet (Bass *et al.*, 2000), while centromeres associate at the opposite nuclear pole and spatially restrict pericentromeric regions from the subtelomeres (Martinez-Perez *et al.*, 2003; Sepsi *et al.*, 2017).

Heat stress has been shown to induce meiotic instability (Draeger & Moore, 2017; Schindfessel *et al.*, 2021; Fu *et al.*, 2022) by delaying CO maturation (De Jaeger-Braet *et al.*, 2022), altering CO positioning and frequency (Higgins *et al.*, 2012; Phillips *et al.*, 2015; Modliszewski *et al.*, 2018) and by disrupting homologous synapsis (De Storme & Geelen, 2020; Ning *et al.*, 2021). Meiotic irregularities result in abnormal gamete formation and infertility (Modliszewski & Copenhaver, 2015; Yang *et al.*, 2021).

Gibberellic acid-insensitive *Rht* alleles are present in a large proportion of modern wheat varieties world-wide. Uncovering the vulnerability of plants carrying GA-insensitive *Rht* alleles is of great interest for crop breeding due to current rising temperatures, which already impose a critical threat to wheat productivity (Asseng *et al.*, 2015; Jacott & Boden, 2020).

Elevated temperatures increase GA levels in the vegetative tissues of GA-insensitive wheats resulting in higher GA levels compared with the WT (Pinthus *et al.*, 1989). Bioactive GAs and functional DELLA proteins are essential for reproductive development in plants (Cheng *et al.*, 2004; Plackett *et al.*, 2014; Jin *et al.*, 2022) and are thus required to ensure fertility. While under optimal temperature conditions GA levels are differentially regulated in the vegetative and the reproductive tissues of the GA-insensitive DELLA mutant wheats (Webb *et al.*, 1998), it is unclear, how early heat stress affects GA concentrations in the floral organs and how it correlates to fertility.

The present study examined the impact of a transient and moderate heat stress applied before the onset of meiosis. Meiosis I and II chromosome segregation and critical early meiotic events of *Rht-B1b* or *Rht-D1b* mutant wheats, including SC formation and recombination, were investigated in detail. Meiotic instability and infertility of *Rht* mutants has been discussed. To understand the effect of heat stress on GA levels in the wheat spike, we studied the transcriptional activity of the *TaGA3ox* gene, encoding the enzyme involved in the last stage of GA biosynthesis. Direct hormone measurements by UPLC-MS elucidated the effect of heat on the bioactive GA products in the developing wheat ear. Implications of our results for future breeding strategies and food security are discussed.

Materials and Methods

Plant material

Seeds of the 'Maris Huntsman' *Rht-B1b*-, *Rht-D1b*- and WT wheat (*Triticum aestivum* L.) near-isogenic lines (accession nos.: W9983, W9984 and W9982, respectively) were provided by the Germplasm Resources Unit of John Innes Centre (Norwich, UK). Near-isogenic lines were tested upon receipt for the *Rht* backgrounds by molecular markers as described by Ellis *et al.* (2002; Supporting Information Fig. S1). Experiments were carried out in growth cabinets at the Phytotron Facility of the Centre for Agricultural Research (ATK, Martonvásár, Hungary, 47°18′51″N, 18°46′57″E, altitude 110 m) in three successive replications in 2019, 2020 and 2021.

Temperature regimes

Following a 6-wk vernalisation period (4°C, 10 h : 14 h, light : dark), plants were potted in 12 cm × 12 cm × 18 cm pots and transferred to a growth cabinet (PGR-15; Conviron, Winnipeg, Manitoba, Canada) following the 'T1' spring programme (Tischner *et al.*, 1997). Plants were transferred to a stress cabinet (PGR-15) when the main shoot entered meiotic interphase (see Methods S1). Heat stress involved a day : night temperature of 30°C for 24 h. Plants were watered twice during heat treatments.

Fertility assessment

Seed set was determined by counting the total number of grains per primary ear. Spikelet number was recorded for each ear analysed, and spikelet fertility was determined by counting the number of grains per spikelet.

Immunolabelling

Anthers were fixed in 4% PFA containing 0.5% (v/v) Igepal CA-630 (18 896; Sigma-Aldrich) for 14 min, the first 5 min involving vacuum infiltration. Meiocytes were slide-mounted and processed as described by Sepsi *et al.* (2018). Primary antibodies applied in the present study included a rabbit antibody raised against the N terminus of the wheat centromeric histone H3 protein (CENH3; Sepsi *et al.*, 2017), a rat anti-ZYP1 antibody (Higgins *et al.*, 2005), a guinea pig anti-ASY1 antibody (Desjardins *et al.*, 2020) and a rabbit anti-γH2AX antibody (H2A.XS139p, C15310223; Diagenode, Belgium, Europe). Primary antibodies

were diluted at a ratio of 1 : 300 (CENH3, ZYP1, γH2AX) and 1 : 1000 (ASY1). The list of secondary antibodies used in this study is presented in Table S1.

In situ hybridisation

The wheat centromeric retrotransposon (CRW; Li *et al.*, 2013) and the universal plant telomeric repeat (TRS; Schwarzacher & Heslop-Harrison, 1991) were amplified by PCR and labelled by nick-translation (AF488 NT Labeling Kit; AF594 NT Labeling Kit; Jena Bioscience, Jena, Germany). *In situ* hybridisation followed the procedure described by Lenykó-Thegze *et al.* (2021) with minor modifications. The hybridisation mix contained 60% (v/v) deionised formamide (F9037; Sigma-Aldrich) and 10% (w/v) dextran sulphate (67 578; Sigma-Aldrich) in 2× SSC (saline-sodium citrate). A volume of 17 µl per slide was completed with 40–60 ng of the labelled probes. The ImmunoFISH procedure was carried out as described by Sepsi *et al.* (2018).

Confocal microscopy

Confocal microscopy was carried out using a TCS SP8 confocal laser scanning microscope (Leica Microsystems GmbH, Wetzlar, Germany). A series of confocal images was obtained using a HC PL APO CS2 639/1.40 oil immersion objective. Full details of confocal imaging are available in Methods S2.

Quantitative reverse transcription-polymerase chain reaction

Total RNA from the excised ears was extracted by using the Qiagen RNeasy plant mini kit after Trizol extraction, with an extra step of DNase treatment programmed in the QIAcube equipment (Qiagen Ltd). The cDNA transcription was performed with 1.0 µg of total RNA using the RevertAid First Strand cDNA synthesis kit (Thermo Fisher Scientific Inc, Waltham, MA, USA). Reverse transcription-polymerase chain reaction (RT-qPCR) was carried out in a Rotor-Gene Q equipment (Qiagen Ltd) applying the SYBR Green technology, as described previously (Kiss *et al.*, 2017).

The *TaGA3ox2* gene has been selected to monitor *TaGA3ox* activities in the developing wheat ears based on its high expression levels in young reproductive tissues (Appleford *et al.*, 2006; Pearce *et al.*, 2011). *TaGA3ox2* gene-specific primers were designed from the conserved regions of cDNA sequences derived from the three genomes of hexaploid wheat (Pearce *et al.*, 2011; Liu *et al.*, 2013). Reference gene *Ta30797* was selected on account of its high stability in temperature treatment analyses of the floral organs (Paolacci *et al.*, 2009). Ears of three plants were pooled for one biological replicate. Three biological replicates were collected, and two technical replicates were used in the analysis.

Droplet digital PCR

Basal and apical ear regions were separately collected to obtain three biological replicates. The ddPCR was performed by using the QX200 Droplet Digital PCR System (Bio-Rad) as described previously (Gulyás *et al.*, 2022). Droplets were prepared by the QX200 Droplet Generator (Bio-Rad) according to the manufacturer's protocol. The water-in-oil emulsions (40 µl) were amplified on an Applied Biosystem Veriti 96 Well (Applied Biosystem, Waltham, MA, USA). Droplets were analysed by the QX200 Droplet Reader and the QuantaSoft software (Bio-Rad) according to the manufacturer's protocol.

Ultra-performance liquid chromatography–tandem mass spectrometry (UPLC-MS/MS)

We developed and validated an in-house method for the most optimal SPE cartridge and conditions as described in Methods S3.

For UPLC separation, a Waters Acquity I class UPLC system (Waters, Milford, MA, USA) was used, and separation was achieved on a Waters Acquity HSS T3 column (1.8 µm, 100 mm × 2.1 mm), kept at 40°C. Mobile phase A was water containing 0.1 v/v % formic acid (FA), while mobile phase B was acetonitrile containing 0.1 v/v % FA. The flow was 0.4 ml min^{-1}, and the gradient profile was as follows: 0 min, 5% B; from 0 to 3 min, linear gradient to 20% B; from 3 to 4.3 min, isocratic 20% B; from 4.3 to 9 min, linear gradient to 45% B; from 9 to 11 min, linear gradient to 100% B; from 11 to 13 min, kept at 100% B; from 13.01 to 15 min, back to the initial conditions of 5% B. The injection volume was 1.5 µl for all samples, which were kept at 8°C in the autosampler during the analysis.

Tandem mass spectrometric detection was performed on a Waters Xevo TQ-XS equipped with a UniSpray™ source (UniSpray Systems, Cambridge, UK) operated in timed multiple reaction monitoring (MRM) mode with the following settings: impactor voltage was 2 kV in both positive and negative modes; nebuliser gas, 6 bar; desolvation temperature, 550°C; cone gas flow, 450 l h^{-1}; desolvation gas flow, 1000 l h^{-1}. For collision gas, argon (5.0 purity) was used with a gas flow of 0.15 ml min^{-1}. Unit resolution was applied to each quadrupole. Dwell time set to be automatically calculated to take at least 20 points across each peak for quantitation. Where possible, at least three MRM transitions were used for data acquisition and the transition having the highest S : N ratio was used for quantitation (Table S2). Data processing was done using Waters MassLynx 4.2 and TargetLynx software. Besides the internal standard, QC samples were also used to verify method performance in each batch to monitor the recovery rates of compounds.

Statistical analyses

Statistical analyses were carried out using the open-source statistical analysis program JASP 0.16 (University of Amsterdam, Amsterdam, the Netherlands). Normality of data was tested by Saphiro–Wilk test, while equality of variances was verified by Levene's test. Figures were produced using the R statistical platform (v.3.6.3) via R studio software (2022.02.0 + 443 'Prairie Trillium'), and the ggplot2 package (3.4.1) was used for visualisation. Further details on the statistical tests are described in Methods S4.

Results

A short period of elevated temperature reduces fertility of *Rht-B1b* and *Rht-D1b* mutants

Elevated temperature resulted in a significantly lower mean seed set per primary spikes for both *Rht-B1b* and *Rht-D1b* lines compared with a nonsignificant decrease in WT (ANOVA, $F(5, 172) = 2377.9$, $\omega^2 = 0.42$, $P < 0.001$; Figs 1a,b, S2). Spikelet number did not vary with genetic background, or the temperature treatments applied in this study (Fig. S3), indicating that reduced spikelet fertility was responsible for the seed set reduction (Fig. 1c; Kruskal–Wallis, Dunn's *post hoc* test, $H(5) = 76.829$, $P < 0.001$). The main spikes of *Rht-B1b* and *Rht-D1b* mutants exhibited a 20% and 31% loss in spikelet fertility. A pronounced effect (40% loss) was detected within the basal region of *Rht-D1b* ears (Fig. 1d,e; Kruskal–Wallis, Dunn's *post hoc* test, $H(5) = 66.899$, $P < 0.001$), whereas the apical region exhibited a 22% reduction (Kruskal–Wallis, Dunn's *post hoc* test, $H(5) = 50.292$, $P < 0.001$). *Rht-B1b* in turn showed a significant but uniform loss of *c.* 20% within both regions (Fig. 1d,e; $P < 0.001$ in both cases). The early reproductive stage of *Rht-B1b* and *Rht-D1b* lines thus exhibits a higher vulnerability to heat stress compared with the WT (tall) line, with the basal region of *Rht-D1b* ears being particularly heat-sensitive.

High temperature increases the frequency of chromosome mis-segregation in *Rht* mutants

To discover whether heat-induced fertility losses may arise from errors in the meiotic process, we investigated the effect of heat

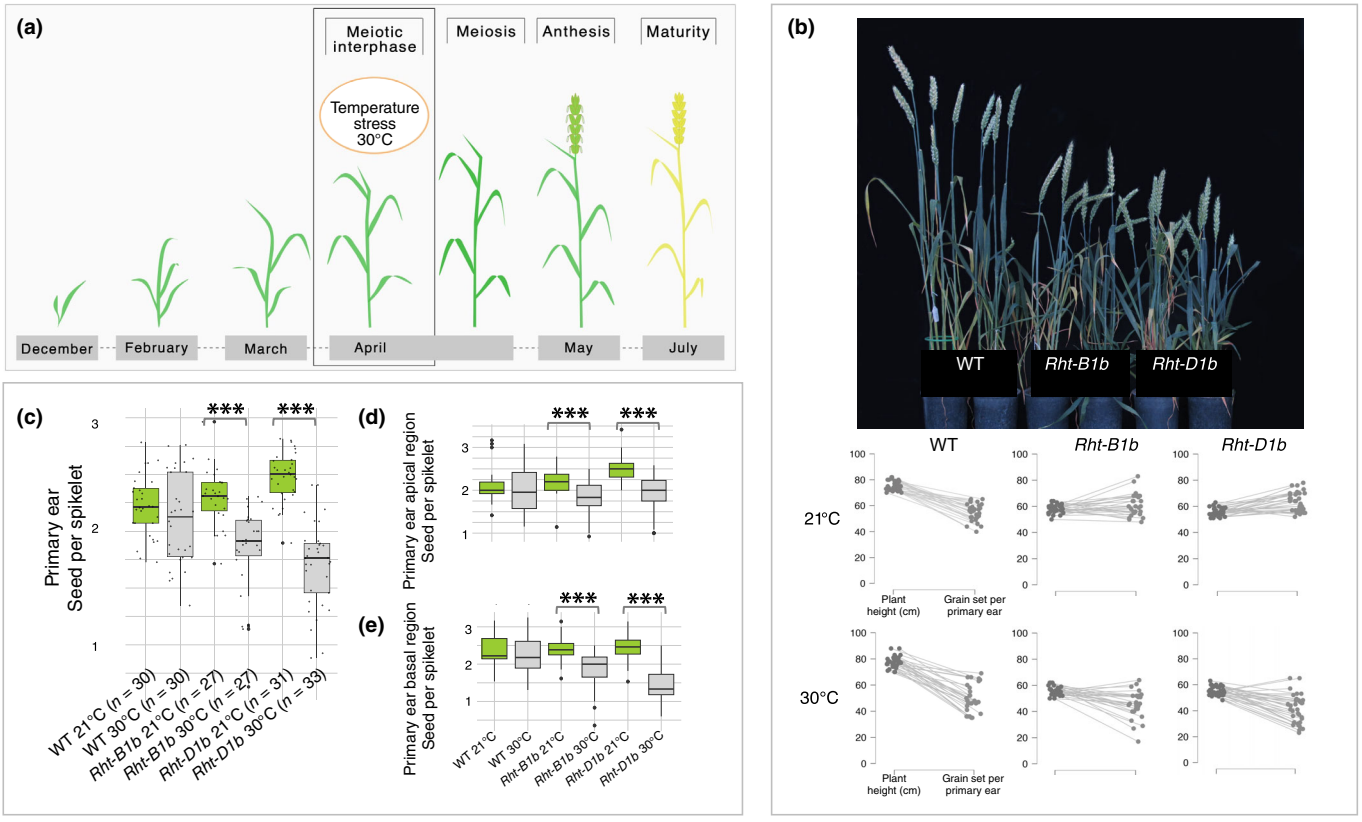

Fig. 1 Effect of heat stress on the fertility of *Rht-B1b* and *Rht-D1b* mutant wheats (semidwarfs) with respect to the wild-type (WT; tall). (a) Schematic representation of the heat stress treatment relative to the developmental stage of bread wheat. Approximate timing of wheat development under Central European field conditions is indicated under the respective developmental stages. Heat stress (30°C) was applied during early reproductive development encompassing the interphase immediately preceding meiotic prophase. At anthesis, natural cross-pollination was prevented by using pollinator bags. Fertility was assessed after grain harvest at full maturity. Artwork has been prepared in Canvas Draw. (b) Seed set is reduced by heat stress in the primary ears of the *Rht-B1b* and *Rht-D1b* semidwarf mutants. Counts of total seeds per primary ears are shown (data points shown on the right side) for each genotype and treatments (21°C and 30°C) together with the corresponding plant heights (cm, data points on the left side). Data points connected by a line originate from the same plant (Statistical analysis shown in Supporting Information Fig. S2). (c) A short period of heat stress (30°C) reduces spikelet fertility (seed per spikelet) within the primary ears of *Rht-B1b* and *Rht-D1b* semidwarf near-isogenic lines ('Maris Huntsman' winter wheat series, see panel (e). Boxplots show counts of seed per spikelet with mean values (horizontal lines) ± SD (whiskers). The number of plants sampled for each line and treatment is shown in brackets. ***, $P < 0.001$ (Kruskal–Wallis test followed by Dunn's *post hoc* test). (d) Heat-treated *Rht-B1b* and *Rht-D1b* wheat lines show similar reduction in spikelet fertility within the apical region of the ears. Counts of seed per spikelet within the apical region of primary ears are presented as mean values ± SD for all three genotypes grown under optimal (20°C) and elevated temperature (30°C) conditions. ***, $P < 0.001$ (Kruskal–Wallis test followed by Dunn's *post hoc* test). (e) Both *Rht-B1b* and *Rht-D1b* show a significant reduction in fertility in the basal region of the primary ears after heat stress, in contrast to the WT. Heat-treated *Rht-D1b* shows a dramatic reduction in fertility within the basal region. Counts of seed per spikelet are presented as mean values ± SD. ***, $P < 0.001$ (Kruskal–Wallis test followed by Dunn's *post hoc* test).

stress on anaphase I and anaphase II chromosome segregation and on genome stability in tetrads and microspores. We combined DAPI counterstaining with CENH3 immunolabelling, which marks functional centromeres (Henikoff, 2001; Houben & Schubert, 2003) and followed chromosome behaviour together with centromere activity.

Wild-type PMCs grown under optimal temperatures revealed balanced homologous chromosome segregation at anaphase I (Fig. 2a), followed by the segregation of the chromatids at anaphase II and meiosis II, which resulted in four sets of chromatids arranged in an isobilateral tetrad configuration (Fig. 2a). Chromosome mis-segregation and chromatin elimination by micronuclei were detected from anaphase I to the early microspore stage in the heat-treated WT, *Rht-B1b* and *Rht-D1b* mutant lines. Unexpectedly, equivalent meiotic errors were detected in the control *Rht-B1b* and *Rht-D1b* meiocytes, although with lower frequencies than in the heat-treated cells. CENH3 immunofluorescence revealed mis-segregating chromosomes equipped with functional centromeres, although random positioning around the bulk chromatin was frequent (Fig. 2a). Analysis of contingency tables followed by chi-squared tests showed unequal incidence of aberrant cells within the investigated WT and *Rht* mutant genotypes and between their respective temperature treatments ($\chi^2(5) = 148.654$, $P < 0.001$). Binomial test revealed that WT male meiocytes exhibited a significantly higher (15%, $P < 0.001$) chromosome mis-segregation under heat stress than under optimal temperature. A similar frequency of aberrant anaphase-telophase I and MII cells occurred within the *Rht-B1b* and *Rht-D1b* controls than the wild treated ($P = 0.373$ and 0.160 vs WT treated, respectively; Fig. 2b; Table S3). *Rht-B1b* and *Rht-D1b* mutants subject to heat stress showed a further increase in the frequency of mis-segregating chromosomes (20%, $P < 0.001$ and 22%, $P < 0.001$, respectively). Cytological analysis on the WT control showed that microspores progressed to the mid-uninucleate stage and produced normal microspores (an eccentric nucleus enclosed by the microspore wall; Fig. 2c), while a higher number of aberrant microspores occurred within the heat-stressed *Rht-B1b* and *Rht-D1b* lines compared with their controls ($\chi^2(5) = 37.416$, $P < 0.001$). Aberrations were manifested as deformed nuclei or as multiple micronuclei located around the main nucleus (Fig. 2c; Table S4). Heat-inferred fertility losses may thus be the result of unbalanced chromosome segregation and programmed

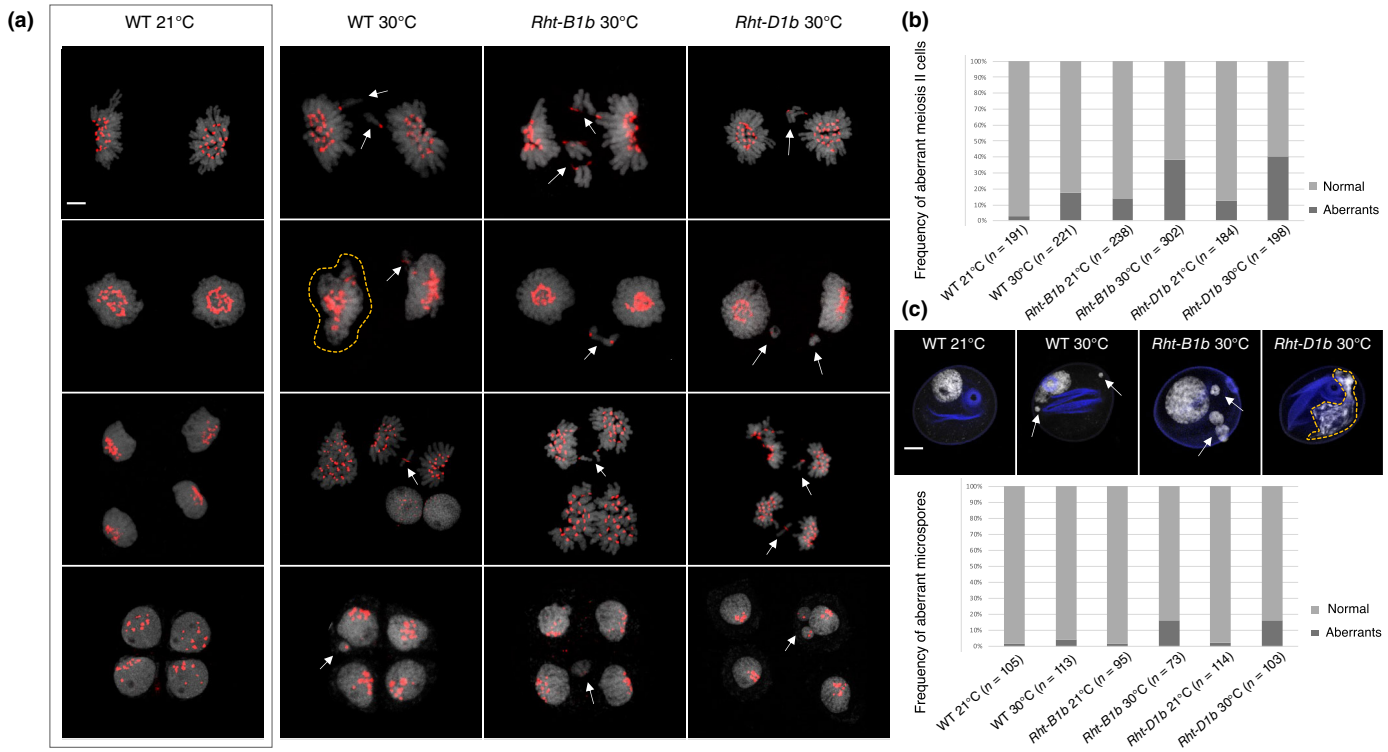

Fig. 2 Heat stress induces a considerable chromosome mis-segregation in *Rht-B1b*, *Rht-D1b* mutant wheat leading to aberrant meiotic products. (a) Meiotic progression of *Rht-B1b*, *Rht-D1b* and wild-type (WT) cells arising from heat-stressed (30°C) or optimal (21°C) temperature conditions. Meiotic stages from top to bottom. Anaphase I, Interphase II, Anaphase II and the tetrad stage. Chromatin is counterstained with 4′,6-diamidino-2-phenylindole (DAPI, grey), and centromere-specific histone H3 (CENH3, red) protein immunofluorescence indicates the location of functional centromeres. Arrows indicate typical examples of lagging chromosomes and chromatin elimination. An amorphous nucleus is circled in yellow. Bars, 5 μm. (b) Frequency of meiotic errors scored from heat-treated and control *Rht-b1b*, *Rht-D1b* and WT meiocytes encompassing stages from anaphase I to tetrads. The number of cells sampled for each line and treatment is shown in brackets. (c) Examples of chromatin fragmentation observed in uninucleate wheat microspores originating from heat stress. Chromatin is shown by DAPI counterstaining (white), and the microspore wall (blue) is visualised by capturing autofluorescence by laser scanning microscopy. Micronuclei are marked with arrows, and an amorph nucleus is encircled in yellow. A representative uninucleate microspore sampled from a WT control plant is presented for comparison. The frequency of aberrant microspores is indicated for each genotype and treatment. The number of cells sampled for each line and treatment is shown in brackets. Bars, 5 μm.

chromatin elimination throughout MII where the frequency of aberrations was significantly higher in the mutants than in the WT.

Rht mutants show a marked reduction in crossover frequency after heat stress

Heat stress is known to affect CO frequency and distribution (Bomblies *et al.*, 2015; Modliszewski & Copenhaver, 2015). We therefore aimed to determine heat-induced changes in CO frequency in *Rht-B1b* and *Rht-D1b* mutant plants by scoring the number of chiasmata per meiotic metaphase I (MI) spread (Sybenga, 1975). *In situ* hybridisation (Schwarzacher *et al.*, 1989), utilising wheat centromeric retrotransposons (CRW; Li *et al.*, 2013) and the TRS (Schwarzacher & Heslop-Harrison, 1991) as probes visualised centromere and telomere positions to show bivalent orientation. Under optimal conditions, WT MI spreads exhibited 51 chiasmata on average (SD = 4.4, $n = 22$), the large majority (92%) of which were ring bivalents (Fig. 3a; Table S5). This did not vary from chiasma frequencies measured in the *Rht-B1b* and *Rht-D1b* control MI cells (*Rht-B1b* $M = 53$, SD = 3.8, $n = 25$; *Rht-D1b* $M = 53$, SD = 4.0, $n = 21$; Kruskal–Wallis, Dunn's *post hoc* test, $H(5) = 78.173$, $P < 0.001$). Heat stress however significantly reduced chiasma number in all three genotypes causing a 12% reduction in the WT ($M = 45$, SD = 8.2, $n = 17$; $P = 0.01$), a loss of 38% in *Rht-B1b* ($M = 33$, SD = 6.2, $n = 21$; $P < 0.001$) and a reduction of 21% in *Rht-D1b* ($M = 42$, SD = 4.6, $n = 18$; $P < 0.001$; Fig. 3a). This was consistent with a significant increase in the number of rod bivalents (Fig. 3a; Table S5; Kruskal–Wallis, Dunn's *post hoc* test, $H(5) = 59.602$, $P < 0.001$). Crossover assurance (Desjardins *et al.*, 2020, 2022; Higgins *et al.*, 2022; Pochon *et al.*, 2022) was impaired, seen in the appearance of univalent chromosomes (Figs 3, S4; Table S5). Contingency tables followed by Chi-squared tests indicated a nonequal incidence of cells with univalent chromosomes within the control and heat-treated meiocytes of the WT, *Rht-B1b* and *Rht-D1b* lines ($\chi^2(5) = 26.452$, $P < 0.001$; Fig. 3a). Binomial tests

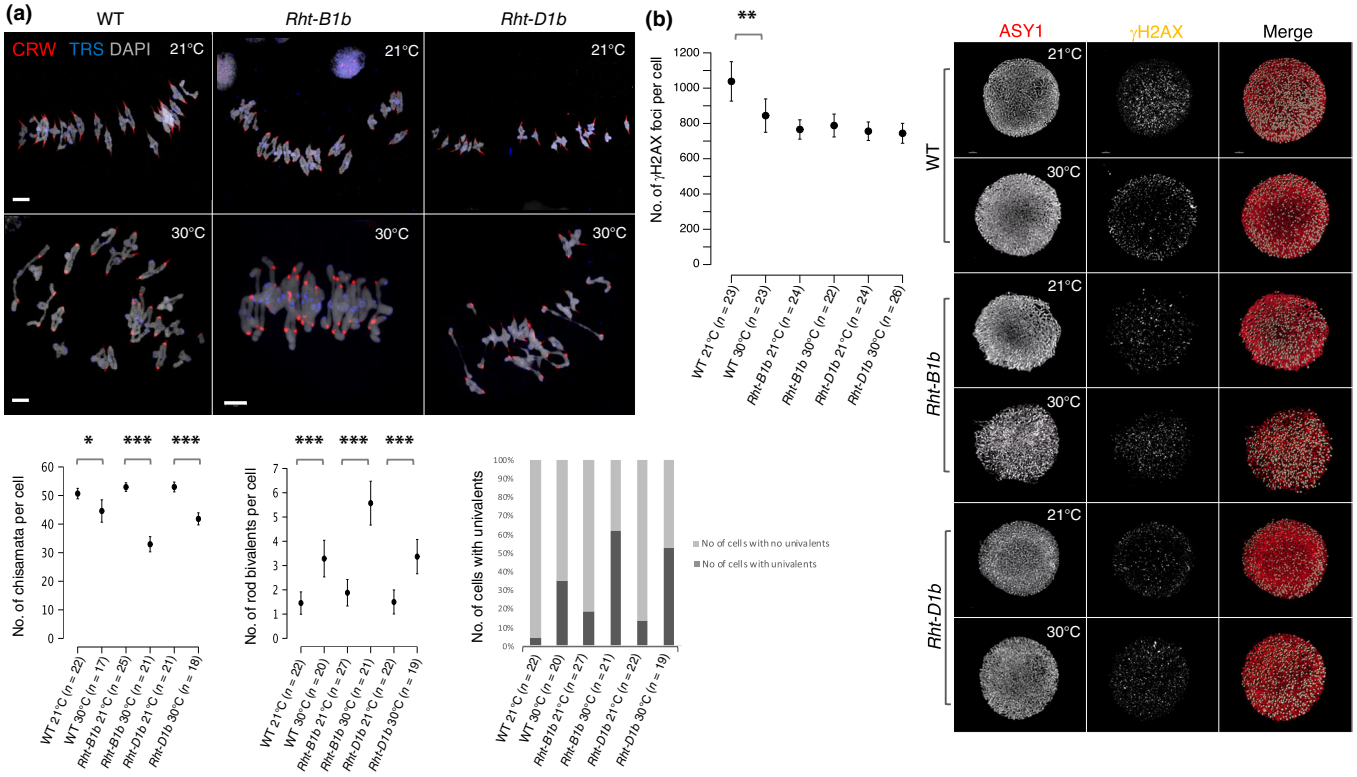

Fig. 3 Effect of heat stress on chiasma frequency and number of double-strand breaks (DSBs) in the *Rht-B1b* and *Rht-D1b* mutant wheats.
(a) Fluorescence *in situ* hybridisation on meiotic metaphase chromosomes of control and heat-treated *Rht-B1b*, *Rht-D1b* and wild-type (WT) plants reveals the location of the centromeres (the wheat centromeric retrotransposon CRW, red) and telomeres (the universal plant telomeric repeat sequence TRS, blue) and together with DAPI counterstaining (grey) identifies chromosome orientation. Bars, 5 μm. Heat stress dramatically reduces the number of chiasmata per cell (presented by an interval plot; dots denote mean values, error bars show ± SD; *, $P = 0.05$; ***, $P < 0.001$) by promoting rod bivalent formation at the expense of ring bivalents (an interval plot shows mean values ± SD; ***, $P < 0.001$) and leads to the loss of obligate chiasmata (univalents) in both *Rht-B1b* and *Rht-D1b* plants. The number of cells carrying univalent chromosomes across the genotypes and treatments used in the study is presented in a bar plot. (b) Co-immunofluorescence labelling of ASY1 protein and γ H2AX foci on *Rht-B1b*, *Rht-D1b* and WT wheat meiocytes collected from optimal and heat-treated conditions. Left panel: The number of DSBs measured in the WT, *Rht-B1b* and *Rht-D1b* meiocytes are presented as mean values (dots) ± SD (error bars). **, $P = 0.01$ (Kruskal–Wallis test followed by Dunn's *post hoc* test). The number of DSBs is reduced following heat stress in the WT but remains unaffected in the *Rht-B1b* and *Rht-D1b* mutants. Right panel: Microscopic images show ASY1 and γH2AX immunosignals in monochrome (first two columns) and pseudocoloured on Merge (red and white, respectively). γH2AX foci are surface rendered on Merge. Bars, 5 μm.

revealed that heat stress significantly increased the frequency of cells carrying univalent chromosomes in all three genotypes (Fig. 3a,b; $P < 0.001$ in all three cases). In addition, meiocytes from *Rht-B1b* and *Rht-D1b* treated plants exhibited a higher frequency of univalents compared with WT ($P < 0.001$; $P = 0.02$, respectively). Reduction in the homologous recombination frequency was accompanied by the occurrence of nonlegitimate connections between the bivalents (Figs 3a, S4, S5). This was clear from poorly spread chromosome conformations connected by thin chromatin bridges, often hindering regular chromosome alignment and centromere biorientation at the equatorial plate (Figs 3a, S4, S5).

Double-strand breaks are unaffected by heat in *Rht-B1b* and *Rht-D1b* mutant wheats

We next investigated whether the heat-induced reduction in chiasma frequency correlated with a lower number of DSBs. DSB quantification was conducted on leptotene nuclei by co-immunofluorescence using anti-TaASY1-antibody as a reliable marker for meiotic timing, and anti-γH2AX antibody marking DSB sites (Fig. 3b; Lang *et al.*, 2012). Heat stress reduced the number of γH2AX loci by 19% in the WT (control $M = 1038$, SD = 274, $n = 23$; heat-treated $M = 844$, SD = 231, $n = 23$; Kruskal–Wallis, $H(5) = 20.567$, Dunn's *post hoc* test, $P = 0.005$). *Rht-B1b* and *Rht-D1b* mutants exhibited a lower number of γH2AX loci (26% and 27% lower, respectively) under optimal temperature compared with the WT control ($P < 0.001$ in both cases). No further decrease was however detected after heat treatment in any of the *Rht* mutants ($P = 0.207$ and 0.482; Fig. 3b). This suggested that normal DELLA proteins are required for the modulation of DSB numbers upon high temperature stress in wheat.

Axial element loading after heat stress in the WT and the *Rht-B1b* and *Rht-D1b* mutants

We sought to investigate whether the reduction in CO number and erroneous chromosome conformations observed at metaphase were associated with errors in chromosome axes. We therefore used immunofluorescence to visualise TaASY1, a protein associated with the meiotic chromosome axes, essential for SC formation and CO assurance (Armstrong *et al.*, 2002; Lambing *et al.*, 2020; Pochon *et al.*, 2022). Pollen mother cells (PMCs) of the WT originating from optimal and elevated temperatures revealed normal AE linearisation at leptotene, gradual ASY1 depletion at zygotene and disappearance of the ASY1 signal from the synapsed axes by pachytene (Fig. S6; Sepsi *et al.*, 2017; Desjardins *et al.*, 2020; Osman *et al.*, 2021). ASY1 loading appeared normal in the mutant lines at 21°C and after heat treatment (Figs 4, 5), but ASY1 could still be observed on a subset of heat-treated *Rht-B1b* and *Rht-D1b* pachytene stage meiocytes colocalising with the synapsed axes (Figs 4b, 5b). Heat stress thus did not affect axis formation in the WT, but the presence of ASY1 on the synapsed axes in pachytene suggested delayed or incomplete protein depletion.

Heat stress perturbs synaptonemal complex formation in *Rht-B1b* and *Rht-D1b*

We next investigated the effects of heat stress on SC polymerisation in the *Rht-B1b* and *Rht-D1b* lines and compared it with WT. Immunofluorescence of ZYP1, the SC transverse filaments protein revealed the nuclear localisation of the SC central element and indicated synapsed chromosomal regions (Higgins *et al.*, 2005). Normal SC morphogenesis in the control WT and *Rht-B1b* meiocytes was evident from subtelomeric SC initiation (Sepsi *et al.*, 2017; Desjardins *et al.*, 2020; Osman *et al.*, 2021) and numerous punctate signals or short ZYP1 segments within the interstitial regions (Figs S6, 4a). These become elongated during mid-zygotene, and synapsis was perfect by pachytene (Figs S6, 4a). Unexpectedly, *Rht-D1b* meiocytes lacked the spatial asymmetry characteristic of early meiosis in cereals (Higgins *et al.*, 2012; Sepsi *et al.*, 2017). Instead, multiple SC initiation points were uniformly distributed in the nucleus, without any visible spatial imbalance, indicating a perturbed meiosis already under control conditions (Fig. 5a).

Heat stress further altered SC formation in both *Rht-B1b* and -*Rht-D1b* mutants. In 65% of the heat-stressed *Rht-B1b* early-zygotene nuclei (number of sampled PMCs are summarised in Table S6), subtelomeric synapsis initiated along with enlarged ZYP1 polycomplexes, while the number of interstitial punctate SC signal was reduced (Fig. 4b). A subset of the sampled *Rht-D1b* early-zygotene nuclei (20%) exhibited equivalent SC initiation defects to *Rht-B1b*, whereas the majority (*c.* 50%) showed a dispersed SC initiation, reminiscent of the *Rht-D1b* controls (Fig. 5a,b). High-resolution microscopy revealed discontinuous SC structures in the heat-treated *Rht-B1b* and *Rht-D1b* PMCs, and to a lesser extent (*c.* 18% of the nuclei) in the WT. Discontinuous SC was evident from mid-zygotene to pachytene, with occasional enlarged ZYP1 polycomplexes (Figs 4b, 5b, S7). Synaptonemal complex (SC) formation thus shows an increased heat-susceptibility in the *Rht-B1b* and *Rht-D1b* lines compared with the WT, most likely due to a genetic predisposition seen by meiotic alterations under optimal conditions.

Rht mutations alter meiotic chromatin dynamics

Synaptonemal complex (SC) emergence in wheat is preceded by a polarised chromatin arrangement, where chromosomes are arranged by their telomeres and centromeres restricted to the two extremes of the nucleus. Telomere polarisation is realised by the formation of the telomere bouquet (Bass *et al.*, 1997; Golubovskaya *et al.*, 2011; Richards *et al.*, 2012), which is coincident with the association of the 42 wheat centromeres into 7–14 groups in the opposite nuclear pole (Martinez-Perez *et al.*, 2003; Sepsi *et al.*, 2017). To reveal whether heat stress affects these chromosome dynamics, we visualised telomere and centromere behaviour during early meiosis by immunofluorescence *in situ* hybridisation (ImmunoFISH) followed by optical sectioning with confocal laser scanning microscopy and 3D rendering. Co-immunofluorescence of the axis protein ASY1 and the centromere-specific histone H3 protein (CENH3) followed by

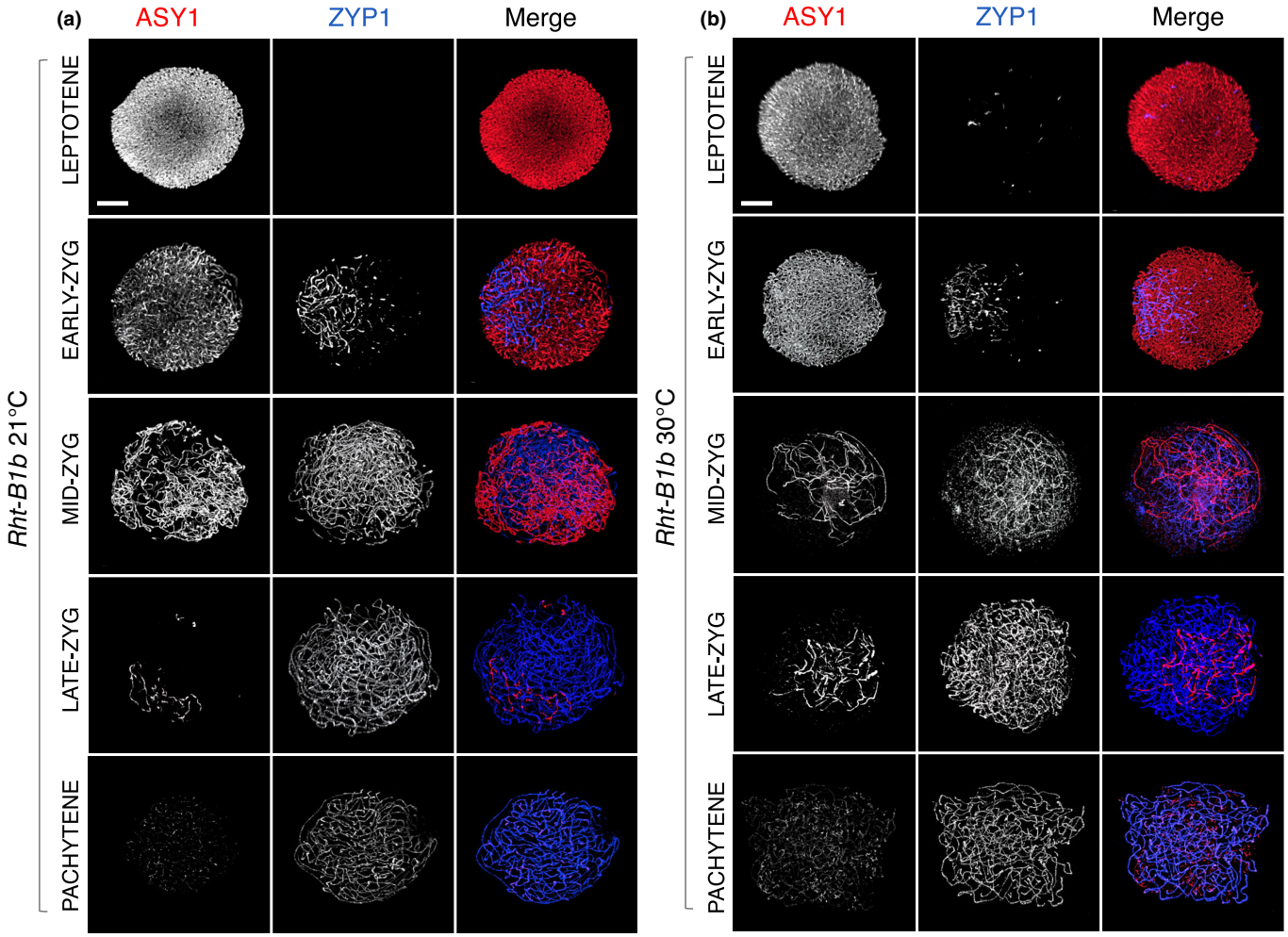

Fig. 4 Axial element (AE) formation and progression of synapsis in meiotic prophase I of control and heat-stressed *Rht-B1b* mutant wheat plants. (a) Co-immunofluorescence of synaptonemal complex (SC) AE protein ASY1 (red) and transverse filament protein ZYP1 (blue) shows linear AEs on the control leptotene meiocytes and marked SC polymerisation from the chromosome ends, forming a conical structure at the nuclear periphery in early-zygotene (Early-Zyg). Proximal chromosomal regions contain multiple ZYP1 foci. ZYP1 lengthening along the chromosome arms occurs from mid-zygotene (Mid-Zyg) to late zygotene (Late Zyg), and synapsis is complete by pachytene. ZYP1 signal is uneven with some regions showing discontinuous threads (Mid-late-zygotene, 21°C). (b) Synapsis initiation is altered in the stressed meiocytes, with very few ZYP1 foci outside the subtelomeric regions (see early-zygotene at 30°C). Noncontinuous ZYP1 axes show abnormal SC structure after heat stress from mid-zygotene to pachytene. Bars, 5 μm.

FISH with TRS showed telomere gathering at the nuclear periphery on late leptotene nuclei of WT plants at both 21°C and 30°C, indicative of normal telomere bouquet formation (Fig. 6). In the meiocytes of the *Rht-B1b* and *Rht-D1b* mutants, a loose telomere gathering appeared at both 21°C and 30°C, with occasional multiple minor telomere associations (Fig. 6). We measured separately nuclear volumes and the volume occupied by the telomeres for each genotype and treatment. Telomeres occupied 5.9% ($n = 23$) and 8.9% ($n = 20$) of the nuclear volumes within the WT control and heat-treated plants, respectively. In *Rht-B1b* control and heat-treated nuclei, telomeres localised within 16.5% ($n = 14$) and 16.3% ($n = 28$) of the nuclear volume. Similarly, telomeres in *Rht-D1b* control and heat-treated plants spread to 15.9% ($n = 21$) and 33.2% ($n = 20$) of the nucleus (Fig. 6), indicating a loose telomere bouquet formation compared with the WT. Regular centromere associations were uncovered at the nuclear periphery in all genotypes and treatments (Fig. 6), which dissolved into the nuclear space by early-mid-zygotene (Fig. S8), as expected (Sepsi *et al.*, 2017). A loose telomere bouquet in the *Rht* mutants is thus coupled with normal centromere dynamics in the mutants, which appears to be insufficient for normal synapsis initiation after heat stress treatment.

A short period of heat stress activates the transcription of GA biosynthesis gene *TaGA3ox* but GA levels remain unaffected

Impaired DELLA protein degradation in GA-insensitive mutants of wheat leads to a marked increase in endogenous GA_1 in the vegetative tissues but not in the developing ears

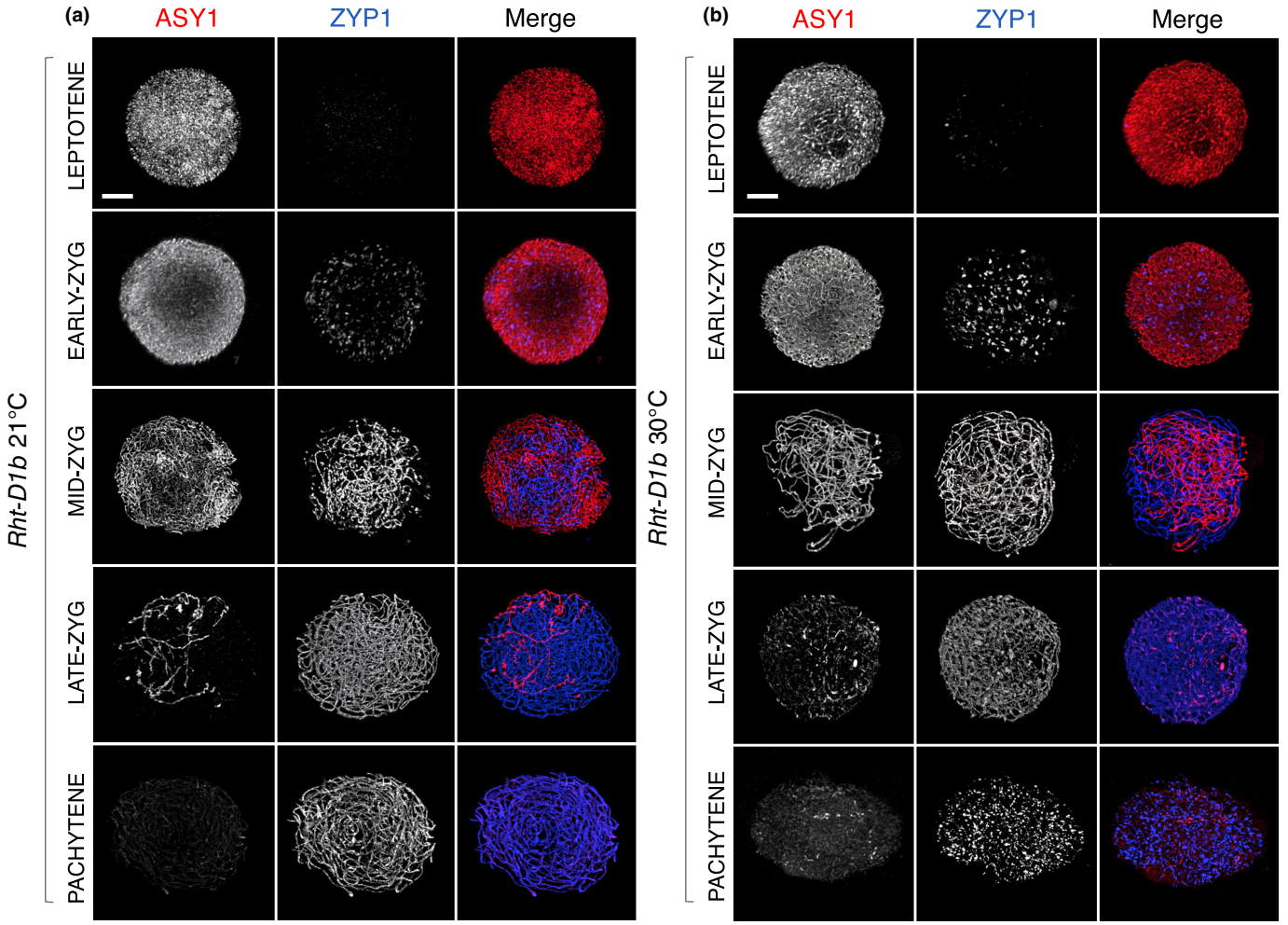

Fig. 5 Axial element (AE) formation and progression of synapsis in meiotic prophase I of *Rht-D1b* mutant control and heat-stressed wheat plants. (a) Co-immunolocalisation of synaptonemal complex (SC) AE protein ASY1 (red) and transverse filament protein ZYP1 (blue). A representative leptotene nucleus shows linear ASY1 signal denoting AEs formed along the chromosomes. In early-zygotene (Early-Zyg), short ZYP1 stretches are dispersed at the periphery of the nucleus indicating SC elongation. Multiple punctate ZYP1 foci are dispersed and indicate additional initiation points. ZYP1 elongates between the chromosome arms from mid-zygotene (Mid-Zyg) to late zygotene (Late Zyg), and synapsis is complete by pachytene. ZYP1 signal is irregular with discontinuous threads (Mid-late-zygotene at 21°C). (b) Synapsis initiation is altered in the stressed *Rht-D1b* meiocytes, with a loss of the characteristic early spatial asymmetry (see dispersed signal on early-zygotene at 30°C). Discontinuous ZYP1 axes show abnormal SC structure after heat stress from mid-zygotene to pachytene. Bars, 5 μm.

(Appleford & Lenton, 1991; Webb *et al.*, 1998). Moreover, elevated temperatures increase bioactive GA levels several fold in the vegetative tissues of GA-insensitive DELLA mutants relative to the WT. Since GA plays a critical role in the meiotic process, we sought to elucidate whether the marked negative effect of heat on the meiotic development of GA-insensitive DELLA mutants may be dependent on GA levels. We therefore measured the effect of a short period of elevated temperature on the final stage of GA biosynthesis and GA levels in the ears of tall and GA-insensitive wheats. We first investigated the transcription of *TaGA 3-oxidase* (*TaGA3ox*) gene encoding the enzyme that catalyses the final reaction of GA biosynthesis (Fig. 7a; Pearce *et al.*, 2015; Barker *et al.*, 2021). RT-qPCR showed significantly increased *TaGA3ox* transcript levels in the ears of each genotype after elevated temperature treatments (Kruskal–Wallis, $H(5) = 30.5$, $P < 0.001$; Dunn's *post hoc* test, WT $P = 0.022$, *Rht-B1b* $P \leq 0.001$ and *Rht-D1b* $P = 0.005$; Fig. 7b). mRNA accumulation was higher within the *Rht-B1b* and *Rht-D1b* mutants (4.7- and 2.3-fold increase, respectively) compared with the WT (2.15-fold increase). Measurement of *TaGA3ox* transcript concentrations between the basal and apical regions of the ears by ddPCR showed a steady transcription along the spike in each genotype under control conditions (Kruskal–Wallis test, $H(11) = 28.2$, $P = 0.003$, Dunn's *post hoc* test: WT $P = 0.166$, *Rht-B1b* $P = 0.454$, *Rht-D1b* $P = 0.176$; Fig. S9). Heat stress significantly increased transcript concentrations in the basal ear region of the WT ($P = 0.017$; Fig. S9) and in both ear regions of *Rht-B1b* ($P = 0.031$ and 0.011, respectively) and *Rht-D1b* ($P = 0.005$ and 0.022, respectively; Fig. S9).

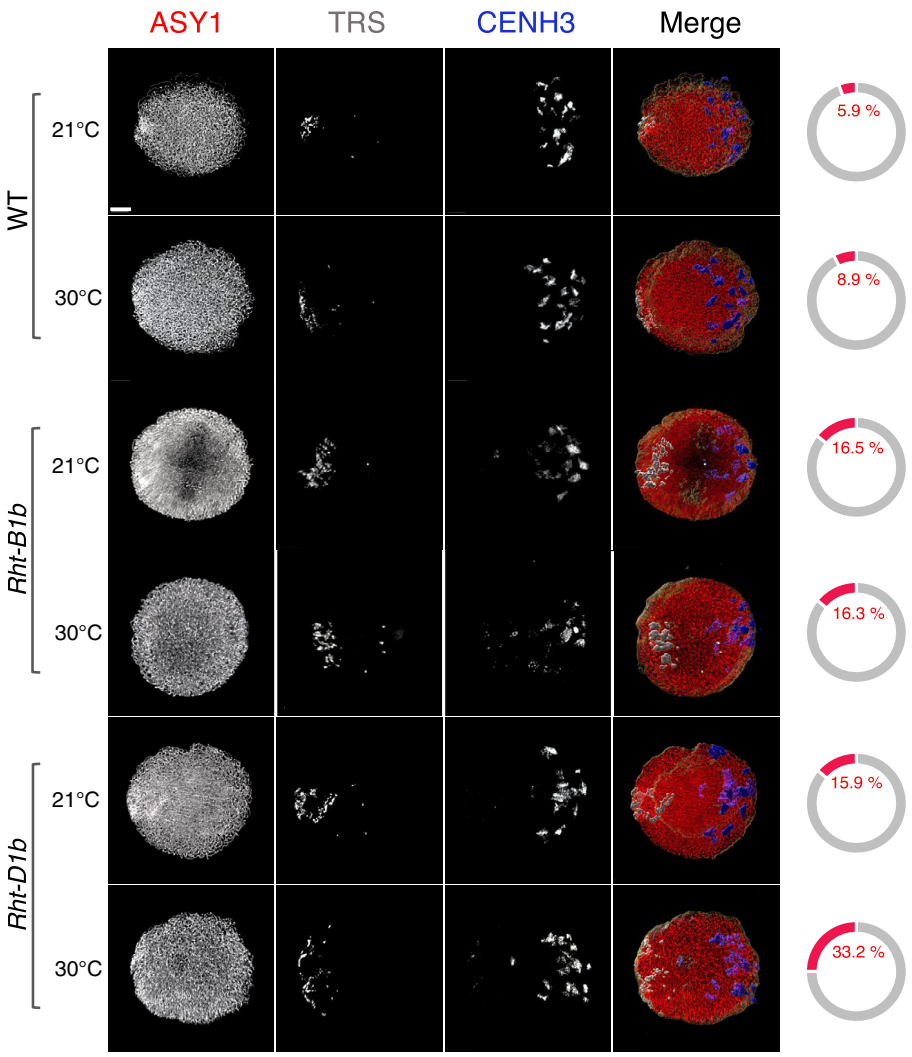

Fig. 6 Deficient telomere bouquet formation in early prophase I of *Rht-B1b* and *Rht-D1b* mutant wheat is coupled with normal centromere dynamics. ASY1 protein labelling (red on merge) allowed the identification of leptotene meiocytes. Simultaneous *in situ* hybridisation with the universal telomeric repeat probe (TRS, white and surface rendered on merged) reveals normal telomere bouquet formation in the control and heat-treated WT pollen mother cells. The control and heat-treated *Rht-B1b* and *Rht-D1b* nuclei displayed a loose bouquet. On the right side of the microscopic images, the percentage of the nuclear volume occupied by the telomeres (red line) is shown with respect to the total nuclear volume (grey line). CENH3 co-immunofluorescence (blue and surface rendered on merge) denotes normal centromere associations at the nuclear periphery in each line and treatment. Bars, 5 μm.

Endogenous GA levels were measured by UPLC-MS–MS and the bioactive GA_1, GA_3 and GA_4, and the inactive forms GA_{20} and GA_8 were quantified using deuterated GAs as internal standards. GA_3 and GA_4 levels remained below 0.5 ng g^{-1} fresh weight (FW) in each genotype and treatment (Fig. 7c; Table S7), indicating that they are not predominant. A similar profile was detected in the GA_1 precursor GA_{20} (< 0.5 ng g^{-1} FW; Fig. 7c; Table S7). Bioactive GA_1 however ranged from 2 to 3 ng g^{-1} FW without showing any significant difference between the genotypes and treatments (Kruskal–Wallis, $H(5) = 7.53$, $P = 0.184$, WT $M = 2.1$ ng g^{-1} FW, *Rht-B1b* $M = 3.1$ ng g^{-1} FW, *Rht-D1b* $M = 2.2$ ng g^{-1} FW). The GA_1 metabolite, GA_8 was present in the ears of all genotypes and showed a minor, nonsignificant decline after heat treatment (Kruskal–Wallis, $H(5) = 15.3$, $P = 0.009$, Dunn's *post hoc* test, WT control vs WT treated $P = 0.06$; *Rht-B1b* control vs *Rht-B1b* treated $P = 0.051$, *Rht-D1b* control vs *Rht-D1b* treated $P = 0.2$). These indicate that in the wheat tissues measured by our analysis heat stress activated the final step of GA biosynthesis but neither the genetic background nor the heat treatment affected GA levels.

Discussion

We imposed a short transient heat stress in a series of controlled-environment experiments and showed that heat applied in the early reproductive stage has a greater effect on the fertility of semidwarf *Rht-B1b* and *Rht-D1b* wheats than on the WT. Our interest resulted from recent warming air temperatures becoming frequent in spring (https://climate.copernicus.eu/dry-and-warm-spring-and-summer), which overlaps the wheat's reproductive cycle. The substantial heat sensitivity of the *Rht-B1b* and *Rht-D1b* mutant wheats shown in the present work was consistent with earlier reports (Borner *et al.*, 1993; Law, 1998); however, the magnitude of negative effects and the causes of their significant heat-induced infertility remained unexplored to date.

Heat reduces crossover frequency but not DSB number in *Rht-B1b* and *Rht-D1b*

In wheat, CO frequency drops significantly between 26°C and 28°C (Coulton *et al.*, 2020) whereas *Arabidopsis* exhibits reduced CO rates between 28°C and 30°C (Lloyd *et al.*, 2018;

New Phytologist

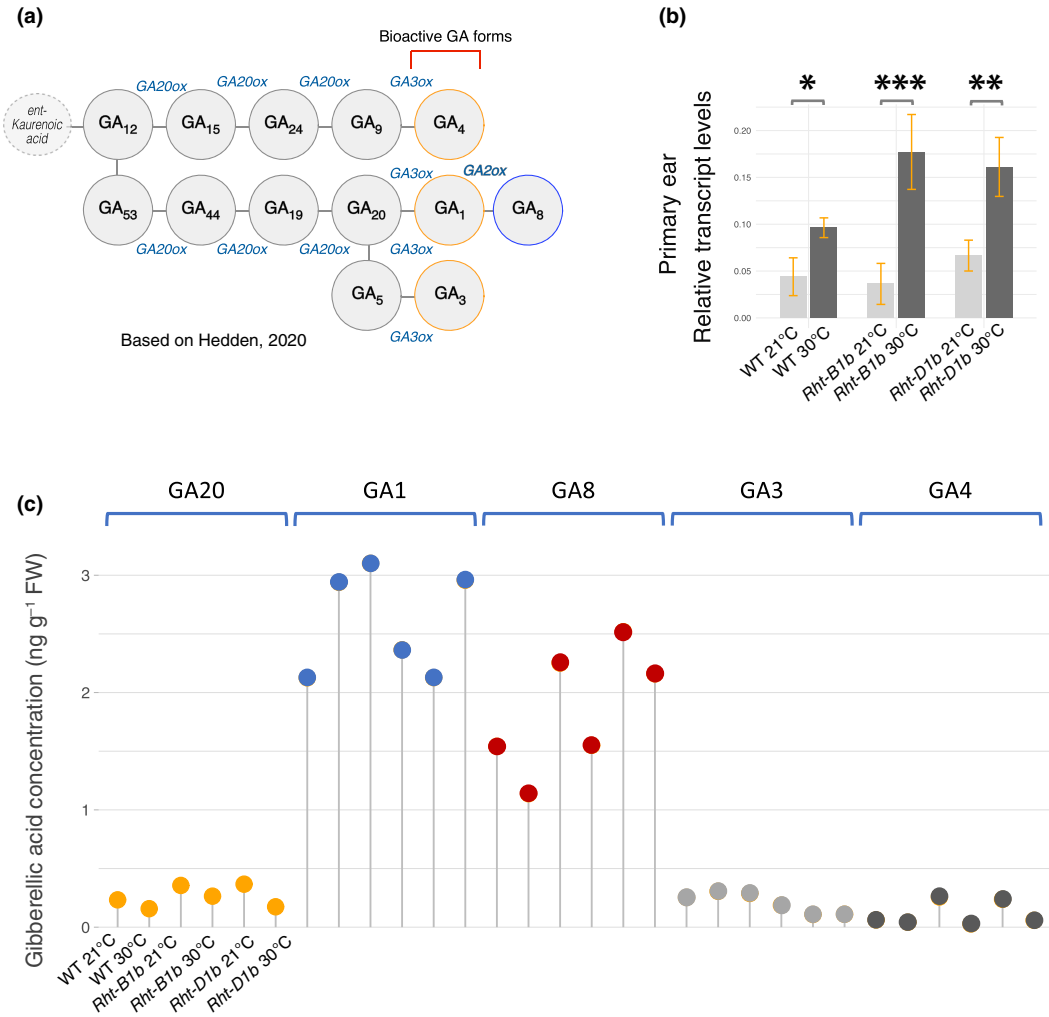

Fig. 7 Gibberellin biosynthesis pathway is activated by heat stress, but endogenous gibberellic acid (GA) levels remain stable following heat treatment. (a) The late stages of the gibberellin biosynthesis pathway (Hedden, 2020). (b) Relative transcript levels reveal a strong activation of the *TaGA3ox* gene after heat stress in the *Rht-B1b* and *Rht-D1b* mutant wheat ears. Measurements are shown as means ± SD (error bars) from three biological replicates. *, $P = 0.05$; **, $P = 0.01$; ***, $P < 0.001$ (Kruskal–Wallis test followed by Dunn's *post hoc* test). (c) Endogenous bioactive gibberellin GA_1, GA_3 and GA_4 concentrations along with concentrations of the GA_1 precursor GA_{20} and the GA_1 metabolite GA_8 in the young developing ears of control and heat-stressed wild-type, *Rht-B1b* and *Rht-D1b* wheat lines. GA_1 is the predominant bioactive gibberellin present in the young developing wheat ears. The levels of GA_1 concentrations did not vary significantly between the different *Rht* genetic backgrounds and between the different temperature treatments applied in the present study. The concentration of GA_8 did not vary significantly after heat treatment. GA3, GA4 and GA20 were present at very low quantities in the young developing wheat ears, irrespective of the genotype and treatment.

Modliszewski *et al.*, 2018; De Storme & Geelen, 2020). In the present study, a transient 30°C heat treatment significantly decreased chiasma frequency in all the wheat genotypes, although *Rht-B1b* and *Rht-D1b* mutants exhibited a considerably greater reduction. Substantial decrease in CO rates was however not associated with a reduction in the number of recombination initiation sites in *Rht-B1b* and *Rht-D1b*, while the number of DSBs appeared to diminish in WT. This suggests an early DELLA-dependent effect in the WT, where recombination may be modulated at DSB initiation. In the mutants, however, that showed a lower number of DSBs under optimal temperatures compared with the WT, recombination is affected at a later stage, possibly during CO designation. While DELLA proteins are critical for reproductive development (Plackett *et al.*, 2014), the molecular pathway through which gibberellin-insensitive DELLA proteins may reduce initial DSB numbers is still unclear. Increasing evidence points to GA-mediated DELLA degradation as a mechanism regulating reproductive development in plants (Cheng *et al.*, 2004; Gomez *et al.*, 2020). Interestingly, fluctuations in DSB numbers are not always reflected in CO frequency (Martini *et al.*, 2006; Cole *et al.*, 2012; Yokoo *et al.*, 2012; Varas *et al.*, 2015) and stable DSB numbers can be contrasted by an increase in Class I COs after a moderate heat treatment (Modliszewski *et al.*, 2018). Final CO rates thus have a limited dependency on DSB numbers but rather become determined during DNA repair, which processes DSBs into COs at the expense or in favour of noncrossovers. DNA repair is increasingly affected by heat stress in *Arabidopsis*, which is reflected in perturbed homologue pairing and SC formation, a recombination-dependent prolongation of the CO maturation process with impaired

resolution of recombination intermediates (De Jaeger-Braet *et al.*, 2022; Zhao *et al.*, 2023). The occurrence of heat-induced nonlegitimate meiotic chromosome connections, as detected in the present work, provides further basis for an altered DSB repair. Chromosome bridges are likely to represent regions in which nonhomologous recombination was initiated but repair prevented or delayed. Heat-inferred ectopic interlinks, indicating promiscuous chromosome interactions, are dependent on SPO11 in *Arabidopsis* (De Storme & Geelen, 2020), the DNA topoisomerase that catalyses DSB formation at the onset of meiotic prophase I (Keeney *et al.*, 1997; Grelon *et al.*, 2001; Da Ines *et al.*, 2020). Heat stress thus perturbs the stringency or the accuracy of homology recognition machinery. Nonhomologous connections are allowed while repair mechanisms appear to fail resolving these connections, leading to a deficient metaphase plate and unbalanced chromosome segregation.

The equatorial position of bivalents and subsequent segregations can be affected by the loss of obligate chiasma (Desjardins *et al.*, 2020), but additional heat-induced negative effects on the microtubule array cannot be overruled. Programmed chromosome elimination was not initiated by centromere inactivity, as micronuclei carried chromatin with still active centromeres. The number of heat-induced meiotic aberrations from anaphase I to the tetrad stage and further to microspore stage indicated that *Rht-B1b* and *Rht-D1b* mutant lines were increasingly affected by meiotic errors than the WT plants.

Heat-induced synaptic events and perturbed chromatin dynamics in *Rht-B1b* and *Rht-D1b* mutants

We explored for the first time in wheat the effects of a moderate heat stress on the localisation and structure of the SC axial and central elements, detected by ASY1 and ZYP1 immunofluorescence. In *A. thaliana*, SC CE assembly is altered at 30–32°C (De Storme & Geelen, 2020; De Jaeger-Braet *et al.*, 2022) whereas AEs become only destabilised at temperatures over the fertile threshold (36–38°C, 24 h; Ning *et al.*, 2021). These are consistent with our findings on WT wheat, where normal chromosome axis was associated with SC disruptions.

Additionally, a disorganised telomere bouquet was linked with an altered synapsis initiation in both heat-treated *Rht* mutant lines, including polycomplex formation and a loss of characteristic spatial asymmetry (Higgins *et al.*, 2012; Sepsi *et al.*, 2017; Osman *et al.*, 2021) in *Rht-D1b*. Polycomplexes represent abnormal SC aggregates and are one of the most frequent heat-induced alterations observed in the SC structure (Loidl, 1989; Higgins *et al.*, 2012; Morgan *et al.*, 2017; Ning *et al.*, 2021; Fu *et al.*, 2022) and have been proposed to result from temperature-inferred denaturation of the SC proteins or prior abnormalities in the chromosome axis (Rog *et al.*, 2017).

The heat-induced dispersed synapsis initiation in the *Rht-D1b* mutants, indicative of disrupted spatial asymmetry, was reminiscent of that observed in barley at temperatures in the range of 30–36°C (Higgins *et al.*, 2012). Unexpectedly, dispersed synapsis initiation and perturbed telomere bouquet appeared in control mutant plants as well. The accumulation of meiotic abnormalities in the heat-treated *Rht-B1b* and *Rht-D1b* plants and the appearance of some of these alterations (although at lower frequencies) under optimal temperature conditions suggested a genetic predisposition for synaptic defects in the *Rht* mutants. A tolerable level of meiotic aberrations occurring under optimal conditions appears to be aggravated by heat stress, rising to a threshold that would have an effect on plant fertility.

Bioactive gibberellin levels are unaffected by the *Rht* mutations and heat stress in the developing wheat ears

In the present study, the activated transcription of *TaGA3ox* gene involved in the final stage of GA biosynthesis was accompanied by stable GA levels. This is in contrast with data collected from the vegetative tissues of GA-insensitive DELLA mutants where GA1 quantities show several fold accumulation vs WT (Fujioka *et al.*, 1988; Talon *et al.*, 1990; Appleford & Lenton, 1991; Webb *et al.*, 1998). Bioactive GA levels thus appear to be differentially regulated between the vegetative and reproductive tissues in cereals (Fig. S10). Although in very low quantities, GA is required for normal meiotic development and fertility (Wilson *et al.*, 1992; Goto & Pharis, 1999; Pearce *et al.*, 2013). High-temperature-induced disrupted early reproductive development has been associated with a reduced (e.g. rice, *Oryza sativa*; Tang *et al.*, 2008; Wu *et al.*, 2016) or an increased GA concentration (e.g. maize, *Zea mays*; Wang *et al.*, 2020) in the reproductive tissues. Stable GA levels however exclude GA fluctuations as a major mediator of heat stress responses in the wheat spike, at least under the short period of high temperature applied in the present study.

We show that the meiotic process, including prophase I events, is markedly affected by heat in wheat carrying truncated DELLAs. DELLA degradation is also required for floral development due to its ability to bind and release transcription factors, thus regulating transcription of target genes (Fu *et al.*, 2002; Cheng *et al.*, 2004; Fukazawa *et al.*, 2021; Jin *et al.*, 2022). Whole-genome microarray analysis following activation of the DELLA paralogue REPRESSOR OF ga1-3 (RGA) in *Arabidopsis* revealed *c.* 800 downregulated and upregulated genes during floral organ development with a considerable number being involved in phytohormone signalling or stress responses (Hou *et al.*, 2008).

A direct effect of DELLA on meiotic process would require local DELLA expression. This is contradicted by evidence from *Arabidopsis* male sporogenesis where the RGA DELLA paralogue is exclusively expressed in the somatic cells surrounding the meiocytes (Liu *et al.*, 2017). A different pattern of DELLA expression appears to emerge however within the members of the *Triticeae*. For instance, the rice DELLA protein SLENDER RICE 1 (SLR1) is expressed in the tapetum and the meiocytes (Hirano *et al.*, 2008; Tang *et al.*, 2010), and transcriptome data from cytologically staged barley meiocytes confirm DELLA expression (Barakate *et al.*, 2021). DELLA protein-encoding genes are also expressed in wheat anthers (Pearce *et al.*, 2011; Van De Velde *et al.*, 2021), although it is to be determined if transcription is present in the meiocytes. These data support that transcriptional regulation by DELLA may affect the expression of meiotic regulators involved in early prophase events. Given the large number

of DELLA targets, DELLA protein expression and degradation allows a rapid response to environmental stimuli by introducing an immediate cell cycle arrest or acceleration, contributing to survival under stress conditions (Cheng *et al.*, 2004; Harberd *et al.*, 2009; Gomez *et al.*, 2020). GA-insensitive truncated DELLA proteins (*Rht* mutants) may affect heat response via their possible accumulation in the floral organs. Permanent repression or activation by DELLA accumulation may reduce the adaptability of important developmental processes. Further studies are needed to identify possible key players in DELLA downstream signalling at meiosis, and its interplay with hormonal networks involved in stress responses and fertility in cereals.

During the present work, the extent of heat stress was specifically selected to model the effects of a single heat wave on the meiotic cell division and fertility of wheat, by focussing on the Green Revolution semidwarf genetic backgrounds, which occur in most of today's wheat cultivars. Our study suggests that under the warming climate, vulnerability of current crop varieties needs to be revisited and addressed globally. Among these, thermotolerance during the period of floral development needs a primary focus, due to the temperature sensitivity of the production of viable gametes. Further research on novel dwarfing genes is urgently needed for the development of new high-yielding genotypes, adaptable to the warmer temperature conditions.

Acknowledgements

We thank Dr John Bailey for linguistic revisions and Dr Mihály Dernovics for his assistance in method optimisation and contribution to sample preparation for the UPLC-MS/MS analysis. Erika Gondos, Barbara Krárné-Péntek and Szilvia Fodor are acknowledged for providing technical assistance. AS and AC acknowledges funding from the Nemzeti Kutatási Fejlesztési és Innovációs Hivatal (NKFIH, NKFI-FK-124266, NKFI-129221, 2021-1.2.4-TÉT-2021-00033). TKP2021-NKTA-06 was implemented with the support provided by the Ministry of Innovation and Technology of Hungary from the National Research, Development and Innovation Fund, financed under the TKP2021-NKTA funding scheme. TK was supported by János Bolyai Research Scholarship of the Hungarian Academy of Sciences (BO/00396/21/4).

Competing interests

None declared.

Author contributions

AS and AC developed the research concept and interpreted the results. AC, TK, ZG, IK and BM carried out molecular biology analyses, KÁH conducted UPLC-MS measurements, AL-T, EM, DM, FS and AS performed cytological experiments. AS wrote the paper.

ORCID

András Cseh https://orcid.org/0000-0002-8681-6654
Zsolt Gulyás https://orcid.org/0000-0003-3072-3528
Kamirán Áron Hamow https://orcid.org/0000-0002-7089-1078
Adél Sepsi https://orcid.org/0000-0003-4473-5490

Data availability

All data supporting the findings of this study are available within the paper and within the supplemental data published online.

References

Appleford NEJ, Evans DJ, Lenton JR, Gaskin P, Croker SJ, Devos KM, Phillips AL, Hedden P. 2006. Function and transcript analysis of gibberellin-biosynthetic enzymes in wheat. *Planta* **223**: 568–582.

Appleford NEJ, Lenton JR. 1991. Gibberellins and leaf expansion in near-isogenic wheat lines containing *Rht1* and *Rht3* dwarfing alleles. *Planta* **183**: 229–236.

Armstrong SJ, Caryl AP, Jones GH, Franklin FCH. 2002. Asy1, a protein required for meiotic chromosome synapsis, localizes to axis-associated chromatin in *Arabidopsis* and *Brassica*. *Journal of Cell Science* **115**: 3645–3655.

Asseng S, Ewert F, Martre P, Rötter RP, Lobell DB, Cammarano D, Kimball BA, Ottman MJ, Wall GW, White JW *et al.* 2015. Rising temperatures reduce global wheat production. *Nature Climate Change* **5**: 143–147.

Barakate A, Higgins JD, Vivera S, Stephens J, Perry RM, Ramsay L, Colas I, Oakey H, Waugh R, Franklin FCH *et al.* 2014. The synaptonemal complex protein ZYP1 is required for imposition of meiotic crossovers in barley. *Plant Cell* **26**: 729–740.

Barakate A, Orr J, Schreiber M, Colas I, Lewandowska D, McCallum N, Macaulay M, Morris J, Arrieta M, Hedley PE *et al.* 2021. Barley anther and meiocyte transcriptome dynamics in meiotic prophase I. *Frontiers in Plant Science* **11**: 619404.

Barker R, Fernandez Garcia MN, Powers SJ, Vaughan S, Bennett MJ, Phillips AL, Thomas SG, Hedden P. 2021. Mapping sites of gibberellin biosynthesis in the *Arabidopsis* root tip. *New Phytologist* **229**: 1521–1534.

Bass HW, Marshall WF, Sedat JW, Agard DA, Cande WZ. 1997. Telomeres cluster *de novo* before the initiation of synapsis: a three-dimensional spatial analysis of telomere positions before and during meiotic prophase. *The Journal of Cell Biology* **137**: 5–18.

Bass HW, Riera-Lizarazu O, Ananiev EV, Bordoli SJ, Rines HW, Phillips RL, Sedat JW, Agard DA, Cande WZ. 2000. Evidence for the coincident initiation of homolog pairing and synapsis during the telomere-clustering (bouquet) stage of meiotic prophase. *Journal of Cell Science* **113**: 1033–1042.

Bayliss MW, Riley R. 1972. An analysis of temperature-dependent asynapsis in *Triticum aestivum*. *Genetical Research* **20**: 193–200.

Bennett MD, Rao MK, Smith JB, Bayliss MW. 1973. Cell development in the anther, the ovule, and the young seed of *Triticum aestivum* L. var. Chinese Spring. *Philosophical Transactions of the Royal Society of London. Series B: Biological Sciences* **266**: 39–81.

Benyahya F, Nadaud I, Da Ines O, Rimbert H, White C, Sourdille P. 2020. SPO11.2 is essential for programmed double-strand break formation during meiosis in bread wheat (*Triticum aestivum* L.). *The Plant Journal* **104**: 30–43.

Bomblies K, Higgins JD, Yant L. 2015. Meiosis evolves: adaptation to external and internal environments. *New Phytologist* **208**: 306–323.

Borner A, Worland AJ, Plaschke J, Schumann E, Law CN. 1993. Pleiotropic effects of genes for reduced height (*Rht*) and day-length insensitivity (*Ppd*) on yield and its components for wheat grown in Middle Europe. *Plant Breeding* **111**: 204–216.

Cheng H, Qin L, Lee S, Fu X, Richards DE, Cao D, Luo D, Harberd NP, Peng J. 2004. Gibberellin regulates *Arabidopsis* floral development via suppression of DELLA protein function. *Development (Cambridge, UK)* **131**: 1055–1064.

Cole F, Kauppi L, Lange J, Roig I, Wang R, Keeney S, Jasin M. 2012. Homeostatic control of recombination is implemented progressively in mouse meiosis. *Nature Cell Biology* **14**: 424–430.

Coulton A, Burridge AJ, Edwards KJ. 2020. Examining the effects of temperature on recombination in wheat. *Frontiers in Plant Science* **11**: 1–13.

Da Ines O, Michard R, Fayos I, Bastianelli G, Nicolas A, Guiderdoni E, White C, Sourdille P. 2020. Bread wheat TaSPO11-1 exhibits evolutionarily conserved function in meiotic recombination across distant plant species. *The Plant Journal* **103**: 2052–2068.

De Jaeger-Braet J, Krause L, Buchholz A, Schnittger A. 2022. Heat stress reveals a specialized variant of the pachytene checkpoint in meiosis of *Arabidopsis thaliana*. *Plant Cell* **34**: 433–454.

De Storme N, Geelen D. 2014. The impact of environmental stress on male reproductive development in plants: biological processes and molecular mechanisms. *Plant, Cell & Environment* **37**: 1–18.

De Storme N, Geelen D. 2020. High temperatures alter cross-over distribution and induce male meiotic restitution in *Arabidopsis thaliana*. *Communications Biology* **3**: 187.

Desjardins SD, Ogle DE, Ayoub MA, Heckmann S, Henderson IR, Edwards KJ, Higgins JD. 2020. *MutS homologue 4* and *MutS homologue 5* maintain the obligate crossover in wheat despite stepwise gene loss following polyploidization. *Plant Physiology* **183**: 1545–1558.

Desjardins SD, Simmonds J, Guterman I, Kanyuka K, Burridge AJ, Tock AJ, Sanchez-Moran E, Franklin FCH, Henderson IR, Edwards KJ *et al.* 2022. FANCM promotes class I interfering crossovers and suppresses class II non-interfering crossovers in wheat meiosis. *Nature Communications* **13**: 1–12.

Draeger T, Moore G. 2017. Short periods of high temperature during meiosis prevent normal meiotic progression and reduce grain number in hexaploid wheat (*Triticum aestivum* L.). *Theoretical and Applied Genetics* **130**: 1785–1800.

Drouaud J, Khademian H, Giraut L, Zanni V, Bellalou S, Henderson IR, Falque M, Mézard C. 2013. Contrasted patterns of crossover and non-crossover at *Arabidopsis thaliana* meiotic recombination hotspots. *PLoS Genetics* **9**: e1003922.

Durand S, Lian Q, Jing J, Ernst M, Grelon M, Zwicker D, Mercier R. 2022. Joint control of meiotic crossover patterning by the synaptonemal complex and HEI10 dosage. *Nature Communications* **13**: 5999.

Ellis MH, Spielmeyer W, Gale KR, Rebetzke GJ, Richards RA. 2002. 'Perfect' markers for the *Rht-B1b* and *Rht-D1b* dwarfing genes in wheat. *TAG. Theoretical and Applied Genetics* **105**: 1038–1042.

Fu H, Zhao J, Ren Z, Yang K, Wang C, Zhang X, Elesawi IE, Zhang X, Xia J, Chen C *et al.* 2022. Interfered chromosome pairing at high temperature promotes meiotic instability in autotetraploid *Arabidopsis*. *Plant Physiology* **188**: 1210–1228.

Fu X, Richards DE, Ait-Ali T, Hynes LW, Ougham H, Peng J, Harberd NP. 2002. Gibberellin-mediated proteasome-dependent degradation of the barley DELLA protein SLN1 repressor. *Plant Cell* **14**: 3191–3200.

Fujioka S, Yamane H, Spray CR, Katsumi M, Phinney BO, Gaskin P, MacMillan J, Takahashi N. 1988. The dominant non-gibberellin-responding dwarf mutant (D8) of maize accumulates native gibberellins. *Proceedings of the National Academy of Sciences* **85**: 9031–9035.

Fukazawa J, Ohashi Y, Takahashi R, Nakai K, Takahashi Y. 2021. DELLA degradation by gibberellin promotes flowering via GAF1-TPR-dependent repression of floral repressors in *Arabidopsis*. *Plant Cell* **33**: 2258–2272.

Golubovskaya IN, Wang CJR, Timofejeva L, Cande WZ. 2011. Maize meiotic mutants with improper or non-homologous synapsis due to problems in pairing or synaptonemal complex formation. *Journal of Experimental Botany* **62**: 1533–1544.

Gomez MD, Barro-Trastoy D, Fuster-Almunia C, Tornero P, Alonso JM, Perez-Amador MA. 2020. Gibberellin-mediated RGA-LIKE1 degradation regulates embryo sac development in *Arabidopsis*. *Journal of Experimental Botany* **71**: 7059–7072.

Goto N, Pharis RP. 1999. Role of gibberellins in the development of floral organs of the gibberellin-deficient mutant, ga1-1, of *Arabidopsis thaliana*. *Canadian Journal of Botany* **77**: 944–954.

Grelon M, Vezon D, Gendrot G, Pelletier G. 2001. AtSPO11-1 is necessary for efficient meiotic recombination in plants. *EMBO Journal* **20**: 589–600.

Gulyás Z, Moncsek B, Hamow KÁ, Stráner P, Tolnai Z, Badics E, Incze N, Darkó É, Nagy V, Perczel A *et al.* 2022. D27-LIKE1 isomerase has a preference towards *trans*/*cis* and *cis*/*cis* conversions of carotenoids in *Arabidopsis*. *The Plant Journal* **112**: 1377–1395.

Harberd NP, Belfield E, Yasumura Y. 2009. The angiosperm gibberellin-GID1-DELLA growth regulatory mechanism: how an "inhibitor of an inhibitor" enables flexible response to fluctuating environments. *Plant Cell* **21**: 1328–1339.

Hartung F, Wurz-Wildersinn R, Fuchs J, Schubert I, Suer S, Puchta H. 2007. The catalytically active tyrosine residues of both SPO11-1 and SPO11-2 are required for meiotic double-strand break induction in *Arabidopsis*. *Plant Cell* **19**: 3090–3099.

Hedden P. 2003. The genes of the Green Revolution. *Trends in Genetics* **19**: 5–9.

Hedden P. 2020. The current status of research on gibberellin biosynthesis. *Plant & Cell Physiology* **61**: 1832–1849.

Henikoff S. 2001. The centromere paradox: stable inheritance with rapidly evolving DNA. *Science* **293**: 1098–1102.

Hesse S, Zelkowski M, Mikhailova EI, Keijzer CJ, Houben A, Schubert V. 2019. Ultrastructure and dynamics of synaptonemal complex components during meiotic pairing and synapsis of standard (A) and accessory (B) rye chromosomes. *Frontiers in Plant Science* **10**: 1–20.

Higgins JD, Osman K, Desjardins SD, Henderson IR, Edwards KJ, Franklin FCH. 2022. Unravelling mechanisms that govern meiotic crossover formation in wheat. *Biochemical Society Transactions* **50**: 1179–1186.

Higgins JD, Osman K, Jones GH, Franklin FCH. 2014. Factors underlying restricted crossover localization in barley meiosis. *Annual Review of Genetics* **48**: 29–47.

Higgins JD, Perry RM, Barakate A, Ramsay L, Waugh R, Halpin C, Armstrong SJ, Franklin FCH. 2012. Spatiotemporal asymmetry of the meiotic program underlies the predominantly distal distribution of meiotic crossovers in barley. *Plant Cell* **24**: 4096–4109.

Higgins JD, Sanchez-Moran E, Armstrong SJ, Jones GH, Franklin FCH. 2005. The *Arabidopsis* synaptonemal complex protein ZYP1 is required for chromosome synapsis and normal fidelity of crossing over. *Genes and Development* **19**: 2488–2500.

Hirano K, Aya K, Hobo T, Sakakibara H, Kojima M, Shim RA, Hasegawa Y, Ueguchi-Tanaka M, Matsuoka M. 2008. Comprehensive transcriptome analysis of phytohormone biosynthesis and signaling genes in microspore/pollen and tapetum of rice. *Plant and Cell Physiology* **49**: 1429–1450.

Hou X, Hu W-W, Shen L, Lee LYC, Tao Z, Han J-H, Yu H. 2008. Global identification of DELLA target genes during *Arabidopsis* flower development. *Plant Physiology* **147**: 1126–1142.

Houben A, Schubert I. 2003. DNA and proteins of plant centromeres. *Current Opinion in Plant Biology* **6**: 554–560.

Hunter N. 2015. Meiotic recombination: the essence of heredity. *Cold Spring Harbor Perspectives in Biology* **7**: 1–35.

Ingvordsen CH, Hendriks P-W, Smith DJ, Bechaz KM, Rebetzke GJ. 2022. Seedling and field assessment of wheat (*Triticum aestivum* L.) dwarfing genes and their influence on root traits in multiple genetic backgrounds. *Journal of Experimental Botany* **73**: 6292–6306.

Jacott CN, Boden SA. 2020. Feeling the heat: developmental and molecular responses of wheat and barley to high ambient temperatures. *Journal of Experimental Botany* **71**: 5740–5751.

Jatayev S, Sukhikh I, Vavilova V, Smolenskaya SE, Goncharov NP, Kurishbayev A, Zotova L, Absattarova A, Serikbay D, Hu Y *et al.* 2020. Green revolution 'stumbles' in a dry environment: dwarf wheat with *Rht* genes fails to produce higher grain yield than taller plants under drought. *Plant, Cell & Environment* **43**: 2355–2364.

Jin Y, Song X, Chang H, Zhao Y, Cao C, Qiu X, Zhu J, Wang E, Yang Z, Yu N. 2022. The GA-DELLA-OsMS188 module controls male reproductive development in rice. *New Phytologist* **233**: 2629–2642.

Keeney S, Giroux CN, Kleckner N. 1997. Meiosis-specific DNA double-strand breaks are catalyzed by Spo11, a member of a widely conserved protein family. *Cell* **88**: 375–384.

Khoo KHP, Able AJ, Able J. 2012. The isolation and characterisation of the wheat molecular ZIPper I homologue, TaZYP1. *BMC Research Notes* **5**: 106.

Kiss T, Dixon LE, Soltész A, Bányai J, Mayer M, Balla K, Allard V, Galiba G, Slafer GA, Griffiths S *et al.* 2017. Effects of ambient temperature in association with photoperiod on phenology and on the expressions of major plant developmental genes in wheat (*Triticum aestivum* L.). *Plant, Cell & Environment* **40**: 1629–1642.

Lambing C, Franklin FCH, Wang C-JR. 2017. Understanding and manipulating meiotic recombination in plants. *Plant Physiology* **173**: 1530–1542.

Lambing C, Kuo PC, Tock AJ, Topp SD, Henderson IR. 2020. ASY1 acts as a dosage-dependent antagonist of telomere-led recombination and mediates crossover interference in *Arabidopsis*. *Proceedings of the National Academy of Sciences, USA* **117**: 13647–13658.

Lang J, Smetana O, Sanchez-Calderon L, Lincker F, Genestier J, Schmit AC, Houlné G, Chabouté ME. 2012. Plant γH2AX foci are required for proper DNA DSB repair responses and colocalize with E2F factors. *New Phytologist* **194**: 353–363.

Law CN. 1998. Sterility in winter wheat: review of occurrence in different varieties and possible causes. *Research Reviews* **44**: 1–107.

Lenykó-Thegze A, Fábián A, Mihók E, Makai D, Cseh A, Sepsi A. 2021. Pericentromeric chromatin reorganisation follows the initiation of recombination and coincides with early events of synapsis in cereals. *The Plant Journal* **107**: 1585–1602.

Li B, Choulet F, Heng Y, Hao W, Paux E, Liu Z, Yue W, Jin W, Feuillet C, Zhang X. 2013. Wheat centromeric retrotransposons: the new ones take a major role in centromeric structure. *The Plant Journal* **73**: 952–965.

Liu A, Gao F, Kanno Y, Jordan MC, Kamiya Y, Seo M, Ayele BT. 2013. Regulation of wheat seed dormancy by after-ripening is mediated by specific transcriptional switches that induce changes in seed hormone metabolism and signaling. *PLoS ONE* **8**: e56570.

Liu B, De Storme N, Geelen D. 2017. Gibberellin induces diploid pollen formation by interfering with meiotic cytokinesis. *Plant Physiology* **173**: 338–353.

Lloyd A, Morgan C, Franklin FC, Bomblies K. 2018. Plasticity of meiotic recombination rates in response to temperature in *Arabidopsis*. *Genetics* **208**: 1409–1420.

Loidl J. 1989. Effects of elevated temperature on meiotic chromosome synapsis in *Allium ursinum*. *Chromosoma* **97**: 449–458.

Lumpkin TA. 2015. How a gene from Japan revolutionized the world of wheat: CIMMYT's quest for combining genes to mitigate threats to global food security. In: Ogihara Y, Takumi S, Handa H, eds. *Advances in wheat genetics: from genome to field*. Berlin, Germany: Springer, 13–20.

Martinez-Perez E, Shaw P, Aragon-Alcaide L, Moore G. 2003. Chromosomes form into seven groups in hexaploid and tetraploid wheat as a prelude to meiosis. *The Plant Journal* **36**: 21–29.

Martini E, Diaz RL, Hunter N, Keeney S. 2006. Crossover homeostasis in yeast meiosis. *Cell* **126**: 285–295.

Mercier R, Mézard C, Jenczewski E, Macaisne N, Grelon M. 2015. The molecular biology of meiosis in plants. *Annual Review of Plant Biology* **66**: 297–327.

Miralles DJ, Calderini DF, Pomar KP, D'Ambrogio A. 1998. Dwarfing genes and cell dimensions in different organs of wheat. *Journal of Experimental Botany* **49**: 1119–1127.

Modliszewski JL, Copenhaver GP. 2015. Meiotic recombination heats up. *New Phytologist* **208**: 295–297.

Modliszewski JL, Wang H, Albright AR, Lewis SM, Bennett AR, Huang J, Ma H, Wang Y, Copenhaver GP. 2018. Elevated temperature increases meiotic crossover frequency via the interfering (Type I) pathway in *Arabidopsis thaliana*. *PLoS Genetics* **14**: e1007384.

Morgan CH, Zhang H, Bomblies K. 2017. Are the effects of elevated temperature on meiotic recombination and thermotolerance linked via the axis and synaptonemal complex? *Philosophical Transactions of the Royal Society of London. Series B: Biological Sciences* **372**: 20160470.

Ning Y, Liu Q, Wang C, Qin E, Wu Z, Wang M, Yang K, Elesawi IE, Chen C, Liu H *et al.* 2021. Heat stress interferes with formation of double-strand breaks and homolog synapsis. *Plant Physiology* **185**: 1783–1797.

Osman K, Algopishi U, Higgins JD, Henderson IR, Edwards KJ, Franklin FCH, Sanchez-Moran E. 2021. Distal bias of meiotic crossovers in hexaploid bread wheat reflects spatio-temporal asymmetry of the meiotic program. *Frontiers in Plant Science* **12**: 1–20.

Osman K, Higgins JD, Sanchez-Moran E, Armstrong SJ, Franklin FCH. 2011. Pathways to meiotic recombination in *Arabidopsis thaliana*. *New Phytologist* **190**: 523–544.

Osman K, Sanchez-Moran E, Higgins JD, Jones GH, Franklin FCH. 2006. Chromosome synapsis in *Arabidopsis*: analysis of the transverse filament protein ZYP1 reveals novel functions for the synaptonemal complex. *Chromosoma* **115**: 212–219.

Paolacci AR, Tanzarella OA, Porceddu E, Ciaffi M. 2009. Identification and validation of reference genes for quantitative RT-PCR normalization in wheat. *BMC Molecular Biology* **10**: 11.

Pearce S, Huttly AK, Prosser IM, Li Y, Vaughan SP, Gallova B, Patil A, Coghill JA, Dubcovsky J, Hedden P *et al.* 2015. Heterologous expression and transcript analysis of gibberellin biosynthetic genes of grasses reveals novel functionality in the GA3ox family. *BMC Plant Biology* **15**: 130.

Pearce S, Saville R, Vaughan SP, Chandler PM, Wilhelm EP, Sparks CA, Al-Kaff N, Korolev A, Boulton MI, Phillips AL *et al.* 2011. Molecular characterization of *Rht-1* dwarfing genes in hexaploid wheat. *Plant Physiology* **157**: 1820–1831.

Pearce S, Vanzetti LS, Dubcovsky J. 2013. Exogenous gibberellins induce wheat spike development under short days only in the presence of VERNALIZATION1. *Plant Physiology* **163**: 1433–1445.

Peng J, Richards DE, Hartley NM, Murphy GP, Devos KM, Flintham JE, Beales J, Fish LJ, Worland AJ, Pelica F *et al.* 1999. 'Green revolution' genes encode mutant gibberellin response modulators. *Nature* **400**: 256–261.

Phillips D, Jenkins G, Macaulay M, Nibau C, Wnetrzak J, Fallding D, Colas I, Oakey H, Waugh R, Ramsay L. 2015. The effect of temperature on the male and female recombination landscape of barley. *New Phytologist* **208**: 421–429.

Phillips D, Nibau C, Wnetrzak J, Jenkins G. 2012. High resolution analysis of meiotic chromosome structure and behaviour in barley (*Hordeum vulgare* L.). *PLoS ONE* **7**: e39539.

Pinthus MJ, Gale MD, Appleford NEJ, Lenton JR. 1989. Effect of temperature on gibberellin (GA) responsiveness and on endogenous GA1 content of tall and dwarf wheat genotypes. *Plant Physiology* **90**: 854–859.

Plackett ARG, Ferguson AC, Powers SJ, Wanchoo-Kohli A, Phillips AL, Wilson ZA, Hedden P, Thomas SG. 2014. DELLA activity is required for successful pollen development in the Columbia ecotype of *Arabidopsis*. *New Phytologist* **201**: 825–836.

Pochon G, Henry IM, Yang C, Lory N, Fernández-Jiménez N, Böwer F, Hu B, Carstens L, Tsai HT, Pradillo M *et al.* 2022. The *Arabidopsis* Hop1 homolog ASY1 mediates cross-over assurance and interference. *PNAS Nexus* **2**: pgac302.

Rebetzke GJ, Verbyla AP, Verbyla KL, Morell MK, Cavanagh CR. 2014. Use of a large multiparent wheat mapping population in genomic dissection of coleoptile and seedling growth. *Plant Biotechnology Journal* **12**: 219–230.

Richards DM, Greer E, Martin AC, Moore G, Shaw PJ, Howard M. 2012. Quantitative dynamics of telomere bouquet formation. *PLoS Computational Biology* **8**: e1002812.

Rog O, Köhler S, Dernburg AF. 2017. The synaptonemal complex has liquid crystalline properties and spatially regulates meiotic recombination factors. *eLife* **6**: 1–26.

Schindfessel C, Drozdowska Z, De Mooij L, Geelen D. 2021. Loss of obligate crossovers, defective cytokinesis and male sterility in barley caused by short-term heat stress. *Plant Reproduction* **34**: 243–253.

Schwarzacher T. 2003. Meiosis, recombination and chromosomes: a review of gene isolation and fluorescent *in situ* hybridization data in plants. *Journal of Experimental Botany* **54**: 11–23.

Schwarzacher T, Heslop-Harrison JS. 1991. *In situ* hybridization to plant telomeres using synthetic oligomers. *Genome* **34**: 317–323.

Schwarzacher T, Leitch AR, Bennett MD, Heslop-Harrison JS. 1989. *In situ* localization of parental genomes in a wide hybrid. *Annals of Botany* **64**: 315–324.

Sepsi A, Fábián A, Jäger K, Heslop-Harrison JS, Schwarzacher T. 2018. ImmunoFISH: simultaneous visualisation of proteins and DNA sequences gives insight into meiotic processes in nuclei of grasses. *Frontiers in Plant Science* **9**: 1193.

Sepsi A, Higgins JD, Heslop-Harrison JSP, Schwarzacher T. 2017. CENH3 morphogenesis reveals dynamic centromere associations during synaptonemal complex formation and the progression through male meiosis in hexaploid wheat. *The Plant Journal* **89**: 235–249.

Sepsi A, Schwarzacher T. 2020. Chromosome–nuclear envelope tethering – a process that orchestrates homologue pairing during plant meiosis? *Journal of Cell Science* **133**: jcs243667.

Sybenga J. 1975. *Meiotic configurations.* Berlin, Germany: Springer.

Talon M, Koornneef M, Zeevaart JAD. 1990. Accumulation of C19-gibberellins in the gibberellin-insensitive dwarf mutantgai of *Arabidopsis thaliana* (L.) Heynh. *Planta* **182**: 501–505.

Tang RS, Zheng JC, Jin ZQ, Zhang DD, Huang YH, Chen LG. 2008. Possible correlation between high temperature-induced floret sterility and endogenous levels of IAA, GAs and ABA in rice (*Oryza sativa* L.). *Plant Growth Regulation* **54**: 37–43.

Tang X, Zhang Z-Y, Zhang W-J, Zhao X-M, Li X, Zhang D, Liu Q-Q, Tang W-H. 2010. Global gene profiling of laser-captured pollen mother cells indicates molecular pathways and gene subfamilies involved in rice meiosis. *Plant Physiology* **154**: 1855–1870.

Tischner T, Kőszegi B, Veisz O. 1997. Climatic programmes used in the Martonvásár phytotron most frequently in recent years. *Acta Agronomica Hungarica* **45**: 85–104.

Van De Velde K, Thomas SG, Heyse F, Kaspar R, Van Der Straeten D, Rohde A. 2021. N-terminal truncated RHT-1 proteins generated by translational reinitiation cause semi-dwarfing of wheat Green Revolution alleles. *Molecular Plant* **14**: 679–687.

Varas J, Sánchez-Morán E, Copenhaver GP, Santos JL, Pradillo M. 2015. Analysis of the relationships between DNA double-strand breaks, synaptonemal complex and crossovers using the *Atfas1–4* mutant. *PLoS Genetics* **11**: 1–29.

Wang H-Q, Liu P, Zhang J-W, Zhao B, Ren B-Z. 2020. Endogenous hormones inhibit differentiation of young ears in maize (*Zea mays* L.) under heat stress. *Frontiers in Plant Science* **11**: 533046.

Webb SE, Appleford NEJ, Gaskin P, Lenton JR. 1998. Gibberellins in internodes and ears of wheat containing different dwarfing alleles. *Phytochemistry* **47**: 671–677.

Wilson RN, Heckman JW, Somerville CR. 1992. Gibberellin is required for flowering in *Arabidopsis thaliana* under short days. *Plant Physiology* **100**: 403–408.

Woglar A, Villeneuve AM. 2018. Dynamic architecture of DNA repair complexes and the synaptonemal complex at sites of meiotic recombination. *Cell* **173**: 1678–1691.

Wu C, Cui K, Wang W, Li Q, Fahad S, Hu Q, Huang J, Nie L, Peng S. 2016. Heat-induced phytohormone changes are associated with disrupted early reproductive development and reduced yield in rice. *Scientific Reports* **6**: 34978.

Wu J, Kong X, Wan J, Liu X, Zhang X, Guo X, Zhou R, Zhao G, Jing R, Fu X *et al.* 2011. Dominant and pleiotropic effects of a GAI gene in wheat results from a lack of interaction between DELLA and GID1. *Plant Physiology* **157**: 2120–2130.

Yang F, Fernández-Jiménez N, Tučková M, Vrána J, Cápal P, Díaz M, Pradillo M, Pecinka A. 2021. Defects in meiotic chromosome segregation lead to unreduced male gametes in *Arabidopsis* SMC5/6 complex mutants. *Plant Cell* **33**: 3104–3119.

Yokoo R, Zawadzki KA, Nabeshima K, Drake M, Arur S, Villeneuve AM. 2012. COSA-1 reveals robust homeostasis and separable licensing and reinforcement steps governing meiotic crossovers. *Cell* **149**: 75–87.

Zhao J, Gui X, Ren Z, Fu H, Yang C, Wang W, Liu Q, Zhang M, Wang C, Schnittger A, Liu B. 2023. ATM-mediated double-strand break repair is required for meiotic genome stability at high temperature. *The Plant Journal* **114**: 403–423.

Zickler D, Kleckner N. 2015. Recombination, pairing, and synapsis of homologs during meiosis. *Cold Spring Harbor Perspectives in Biology* **7**: 2.

Supporting Information

Additional Supporting Information may be found online in the Supporting Information section at the end of the article.

Fig. S1 Molecular and phenotypical characterisation of the wild-type, *Rht-B1b* and *Rht-D1b* Maris Huntsman wheat near-isogenic lines.

Fig. S2 Seed set in the primary ears of the wild-type, *Rht-B1b* and *Rht-D1b* semidwarf mutant wheats under control and heat stress conditions.

Fig. S3 Spikelet number is stable within the wild-type, *Rht-B1b* and *Rht-D1b* mutant wheat ears.

Fig. S4 Representative micrographs of heat-treated wild-type, *Rht-B1b* and *Rht-D1b* mutant wheat male meiotic metaphase I spreads.

Fig. S5 Enlargements of micrographs presented in Fig. S4.

Fig. S6 Axial element formation and progression of synapsis in the control and heat-treated wild-type wheat plants.

Fig. S7 Representative single-section enlargements from *z*-series of immunolabelled wild-type, *Rht-B1b* and *Rht-D1b* mutant wheat pollen mother cells.

Fig. S8 ASY1 and CENH3 co-immunofluorescence reveals the progression of normal centromere dynamics in zygotene pollen mother cells of control and heat-stressed *Rht-B1b* and *Rht-D1b* wheat plants.

Fig. S9 Droplet Digital PCR analysis of the activity of *TaGA3ox* gene in the basal and apical regions of wheat spike.

Fig. S10 Schematic representation of the effects of gibberellic acid-insensitive DELLA mutation on DELLA protein degradation and endogenous gibberellic acid levels in wheat.

Methods S1 Meiotic staging of wheat spikes prior heat stress treatment.

Methods S2 Confocal microscopy.

Methods S3 Sample preparation for ultra-performance liquid chromatography–tandem mass spectrometry.

Methods S4 Statistical methods.

Table S1 List of secondary antibodies used in the present study.

Table S2 Retention time and multiple reaction monitoring transitions used for qualitative and quantitative determination of target compounds by UPLC-US-MS/MS.

Table S3 Number of wheat meiocytes carrying mis-segregating chromosomes or micronuclei vs meiocytes with normal meiotic progression in the control and heat-treated wild-type, *Rht-B1b* and *Rht-D1b* mutant wheat plants.

Table S4 Number of aberrant and normal uninucleate microspores detected in the control (21°C) and treated (30°C) wild-type and *Rht-B1b* and *Rht-D1b* mutant wheat lines.

Table S5 Mean number of metaphase I chromosome conformations in the sampled control and heat-stressed wild-type, *Rht-B1b* and *Rht-D1b* mutant wheat meiocytes.

Table S6 Number of prophase I wheat meiocytes sampled for synaptonemal complex immunofluorescence.

Table S7 Descriptive statistics of gibberellic acid levels ($ng\,g^{-1}$ fresh weight) measured by UPLC-MS in the control (21°C) and treated (30°C) wild-type, *Rht-B1b* and *Rht-D1b* wheat ears.

Please note: Wiley is not responsible for the content or functionality of any Supporting Information supplied by the authors. Any queries (other than missing material) should be directed to the *New Phytologist* Central Office.